FINAL REPORT

FHWA-WY-16/02F

State of Wyoming
Department of Transportation

U.S. Department of Transportation
Federal Highway Administration

IMPLEMENTATION AND LOCAL CALIBRATION OF THE MEPDG TRANSFER FUNCTIONS IN WYOMING

By:
Applied Research Associates, Inc.
100 Trade Center Drive, Suite 200
Champaign, IL, 61820

November 2015

Notice

This document is disseminated under the sponsorship of the Wyoming Department of Transportation (DOT) and the U.S. Department of Transportation in the interest of information exchange. The Wyoming DOT and U.S. Government assume no liability for the use of the information contained in this document. This report does not constitute a standard, specification, or regulation.

The Wyoming DOT or U.S. Government does not endorse products or manufacturers. Trademarks or manufacturers' names appear in this report only because they are considered essential to the objective of the document.

Quality Assurance Statement

The Wyoming DOT and Federal Highway Administration (FHWA) provide high-quality information to serve Government, industry, and the public in a manner that promotes public understanding. Standards and policies are used to ensure and maximize the quality, objectivity, utility, and integrity of its information. Wyoming DOT the FHWA periodically review quality issues and adjusts its programs and processes to ensure continuous quality improvement.

TECHNICAL DOCUMENTATION PAGE

1. Report No. FHWA 16/02F	2. Government Accession No.	3. Recipient's Catalog No.
4. Title and Subtitle Implementation and Local Calibration of the MEPDG Transfer Functions in Wyoming		5. Report Date November 6, 2015 6. Performing Organization Code
7. Author(s) Biplab B. Bhattacharya, P.E., Harold L. Von Quintus, P.E., and Michael I. Darter, Ph.D., P.E.		8. Performing Organization Report No.
9. Performing Organization Name and Address Applied Research Associates, Inc. 100 Trade Centre Blvd., Suite #200 Champaign, Illinois 61820		10. Work Unit No. (TRAIS) 11. Contract or Grant No. RS03209
12. Sponsoring Agency Name and Address Wyoming Department of Transportation 5300 Bishop Blvd. Cheyenne, Wyoming 82009-3340		13. Type of Report and Period Covered Final Calibration Report August 2014 to November 2015 14. Sponsoring Agency Code

15. Supplementary Notes
The Contracting Officer's Technical Representative (COTR) was Mr. Bob Rothwell

16. Abstract
The Wyoming Department of Transportation (WYDOT) currently uses the empirical AASHTO Design for Design of Pavement Structures as their standard pavement design procedure. WYDOT plans to transition to the Mechanistic Empirical Pavement Design Guide (MEPDG) for designing new and rehabilitated highway pavements. As a part of the transitioning process, WYDOT has sponsored an implementation project. One part of the implementation project is to verify the MEPDG global distress transfer functions and calibrate these functions to local conditions, if determined to be necessary. The Wyoming Long-Term Pavement Performance (LTPP) and non-LTPP roadway segments, as well as LTPP test section is adjacent states were used for this verification-calibration process.

As noted above, one objective of the implementation project was to verify or confirm that the MEPDG transfer functions and global calibration coefficients derived from NCHRP project 1-40D reasonably predict distresses and smoothness in Wyoming. One of the tasks within this project focused on using the Wyoming LTPP test sections to confirm the applicability of the global calibration coefficients. Results from the initial verification concluded some of the transfer functions exhibited significant bias between the measured and predicted distress and require local calibration. Thus, some of the LTPP test sections in adjacent states with similar design features built in Wyoming combined with some non-LTPP roadway segments in Wyoming were used to determine the coefficients of the transfer functions to eliminate any bias between the measured and predicted distresses.

This report documents the local calibration of the transfer functions using LTPP and non-LTPP roadway segments. The calibration process follows the steps presented in the 2010 AASHTO MEPDG Local Calibration Guide. Local calibration coefficients were derived to remove that bias for the rutting, fatigue cracking, and thermal cracking transfer functions of flexible pavements, and the faulting and fatigue cracking transfer functions of rigid pavements. The global coefficients of the smoothness degradation regression equation for flexible and rigid pavements were also checked for their applicability to Wyoming conditions.

17. Key Words Mechanistic-Empirical Pavement Design Guide, ME Design, Transfer Functions, Fatigue Cracking, Rutting, Thermal Cracking, Faulting, Mid-Slab Cracking, IRI, Wyoming		18. Distribution Statement No restrictions.	
19. Security Classification of this report: Unclassified	20. Security Classification (of this page): Unclassified	21. No. of Pages 70	22. Price

Form DOT F 1700.7 (8-72) Reproduction of completed page authorized

SI* (MODERN METRIC) CONVERSION FACTORS

APPROXIMATE CONVERSIONS TO SI UNITS

Symbol	When You Know	Multiply By	To Find	Symbol
		LENGTH		
in	inches	25.4	millimeters	mm
ft	feet	0.305	meters	m
yd	yards	0.914	meters	m
mi	miles	1.61	kilometers	km
		AREA		
in^2	square inches	645.2	square millimeters	mm^2
ft^2	square feet	0.093	square meters	m^2
yd^2	square yard	0.836	square meters	m^2
ac	acres	0.405	hectares	ha
mi^2	square miles	2.59	square kilometers	km^2
		VOLUME		
fl oz	fluid ounces	29.57	milliliters	mL
gal	gallons	3.785	liters	L
ft^3	cubic feet	0.028	cubic meters	m^3
yd^3	cubic yards	0.765	cubic meters	m^3
	NOTE: volumes greater than 1000 L shall be shown in m^3			
		MASS		
oz	ounces	28.35	grams	g
lb	pounds	0.454	kilograms	kg
T	short tons (2000 lb)	0.907	megagrams (or "metric ton")	Mg (or "t")
		TEMPERATURE (exact degrees)		
^oF	Fahrenheit	5 (F-32)/9 or (F-32)/1.8	Celsius	^oC
		ILLUMINATION		
fc	foot-candles	10.76	lux	lx
fl	foot-Lamberts	3.426	$candela/m^2$	cd/m^2
		FORCE and PRESSURE or STRESS		
lbf	poundforce	4.45	newtons	N
lbf/in^2	poundforce per square inch	6.89	kilopascals	kPa

APPROXIMATE CONVERSIONS FROM SI UNITS

Symbol	When You Know	Multiply By	To Find	Symbol
		LENGTH		
mm	millimeters	0.039	inches	in
m	meters	3.28	feet	ft
m	meters	1.09	yards	yd
km	kilometers	0.621	miles	mi
		AREA		
mm^2	square millimeters	0.0016	square inches	in^2
m^2	square meters	10.764	square feet	ft^2
m^2	square meters	1.195	square yards	yd^2
ha	hectares	2.47	acres	ac
km^2	square kilometers	0.386	square miles	mi^2
		VOLUME		
mL	milliliters	0.034	fluid ounces	fl oz
L	liters	0.264	gallons	gal
m^3	cubic meters	35.314	cubic feet	ft^3
m^3	cubic meters	1.307	cubic yards	yd^3
		MASS		
g	grams	0.035	ounces	oz
kg	kilograms	2.202	pounds	lb
Mg (or "t")	megagrams (or "metric ton")	1.103	short tons (2000 lb)	T
		TEMPERATURE (exact degrees)		
^oC	Celsius	1.8C+32	Fahrenheit	^oF
		ILLUMINATION		
lx	lux	0.0929	foot-candles	fc
cd/m^2	$candela/m^2$	0.2919	foot-Lamberts	fl
		FORCE and PRESSURE or STRESS		
N	newtons	0.225	poundforce	lbf
kPa	kilopascals	0.145	poundforce per square inch	lbf/in^2

*SI is the symbol for the International System of Units. Appropriate rounding should be made to comply with Section 4 of ASTM E380.
(Revised March 2003)

TABLE OF CONTENTS

LIST OF FIGURES

Figure Number **Page No.**

LIST OF TABLES

Table Number **Page No.**

CHAPTER 1 — INTRODUCTION

1.3 Background

Many highway agencies, including the Wyoming Department of Transportation (WYDOT), are transitioning from empirical design procedures to the Mechanistic-Empirical Pavement Design Guide (MEDPG) procedure for designing new and rehabilitated pavements (AASHTO, 2008). The MEPDG is a part of the American Association of State Highway and Transportation Officials (AASHTO) software *Pavement ME Design*® version 2.2 and uses mechanistic-empirical (ME) principles (AASHTO, 2015). This procedure is a significant departure from the existing empirical procedures (such as the 1972 and 1993 AASHTO procedures).

The MEPDG distress transfer functions and prediction methodology were calibrated using data from the Long Term Pavement Performance (LTPP) program under National Cooperative Highway Research Program (NCHRP) projects 1-37A and 1-40D (NCHRP, 2004 and 2006). A transfer function is defined as a mathematical relationship that transfers computed mechanistic pavement responses (stresses, strains, and/or deflections) into what is observed or measured on the pavement surface.

The global calibration effort, however, cannot consider all potential factors that can occur throughout all agencies in North America. Factors such as maintenance strategies, construction specifications, aggregate and binder type, mixture design procedures, and material specifications can result in performance differences – all other factors being equal. In fact, small differences in some of the above factors can cause large differences in performance.

The overall objective of WYDOT's implementation process was to validate and re-calibrate, if necessary, the transfer functions. In other words, adjusting the distress and smoothness prediction models or transfer functions so that they accurately represent the performance of WYDOT roadways. Local calibration will enable WYDOT to use the MEPDG with confidence for the design of new and rehabilitated pavements.

1.2 Objective

The objective of the implementation effort was to determine the MEPDG transfer function calibration coefficients to eliminate any bias between the measured and predicted distress values. The calibration process followed the procedure presented in the AASHTO MEPDG Local Calibration Guide (AASHTO, 2010). This report documents use of the LTPP sites in Wyoming and in adjacent states and non-LTPP sites in Wyoming to determine the Wyoming derived calibration coefficients to accurately predict distress and smoothness.

1.3 Scope of Work

As stated above, it is impossible to account for all factors in developing a global distress/performance simulation model. All models have errors because of simplifying assumptions, so it is good practice to evaluate the applicability of any conceptual and/or statistical model on a limited basis prior to full-scale use.

Local calibration of the MEPDG distress transfer function coefficients and standard deviations of the transfer functions for Wyoming conditions was completed in accordance with the AASHTO MEPDG Local calibration Guide (AASHTO, 2010). This procedure is a four-part process divided into multiple steps. The four major parts of the process included:

1. Determining the inputs for the calibration pavement sections.
2. Verify the global calibration coefficients for each transfer function by executing the *Pavement ME Design*® software using the global calibration coefficients and evaluate the goodness-of-fit and bias for the calibration sections.
3. If significant bias is found, modify or adjust the coefficients of the transfer function to eliminate any bias and reduce the standard error of the estimate (SEE) or standard deviation between the predicted and measured values. In addition, determine whether the adjustment to the coefficients is dependent on some design feature or material/layer property.
4. Verify the resulting calibration coefficients for each transfer function by executing the *Pavement ME Design*® software using the local or adjusted global calibration coefficients for the calibration sections and evaluate the goodness-of-fit and bias.

CHAPTER 2 — TEST SECTIONS USED IN CALIBRATION PROCESS

The distress transfer functions and International Roughness Index (IRI) regression equations were calibrated using a wide range of pavement sections located across North America. Global models, however, require confirmation at the local level to ensure their accuracy and unbiasedness to local conditions and operational or management policies. This section of the report identifies the roadway segments used to determine the Wyoming calibration coefficients.

2.1 LTPP Test Sections

The LTPP sections located in Wyoming were initially planned for use as the primary data set for the verification-calibration process. However, only 9 flexible pavement sections, 13 semi-rigid pavement sections, and 1 rigid pavement section are included in the LTPP database. These Wyoming LTPP sections represent an insufficient number of sites for calibration. As such, selected LTPP sections located near the state-line of adjacent states were used for the verification-calibration process. The additional LTPP sites were selected that have similar pavement characteristics and site conditions found in Wyoming.

Figure 1 shows the location and geographic distribution of the LTPP sites in Wyoming and adjacent states. Tables 1 and 2 list the LTPP flexible and rigid pavement sections, respectively, and generally represent past WYDOT design practices and material specifications. Most of these LTPP sites in adjacent states, as related to local calibration, are discussed in detail in other reports (Bayomy, et al., 2011; Darter, et al., 2009; Mallela, et al., 2013; Von Quintus and Moulthrop, 2007).

Some design features and policies used in Wyoming were excluded and/or inadequately represented by these LTPP sites. The following summarizes the items that can have a significant impact on pavement performance but were excluded as features/factors in the Wyoming LTPP verification-calibration test sections.

- Polymer modified asphalt (PMA) mixtures. PMA mixtures are used in Wyoming on interstate or higher volume roadways, while neat (unmodified) mixtures are used in lower volume roadways. None of the LTPP sections include PMA mixtures. Multiple studies, however, have concluded that PMA mixtures provide enhanced performance which is not properly accounted for by the MEPDG distress prediction methodology (Von Quintus, et al., 2007).

- Hot mix asphalt (HMA) mixtures with higher recycled asphalt pavement (RAP) contents. WYDOT allows RAP in their mixtures, which can have an impact on the fracture and fatigue properties. There were an insufficient number of LTPP sections with and without RAP to determine the impact (positive or negative) on pavement cracking and performance.

- Pavement preservation treatments were not included on any of the LTPP test sections for both types of pavements. Calibration of the MEPDG should consider or include this benefit, but the MEPDG does not have the capability to directly consider the

impact of different pavement preservation methods. Most preservation methods do not add structural value to the existing pavement. Thus, another confounding factor is pavement preservation because of the potential difference in performance between LTPP and non-LTPP sections.

The Montana Department of Transportation (MDOT) is the only agency where pavement preservation methods were considered within the calibration process to date (Von Quintus and Moulthrop, 2007). It is expected that a similar type of procedure be used to eliminate bias in the predictions of distress and consider the impact of preservation methods on enhancing performance. Michigan DOT is identifying methods to account for or consider the benefit of using aggressive preservation programs in terms of the MEPDG (Von Quintus and Perera, 2011). Arizona DOT has sufficient performance data on preservation methods and investigated how that data can be used to adjust or determine their local calibration coefficients (Darter, et al., 2014). The key issue is how to determine the standard error of the estimate when these methods are placed at different times under different existing pavement conditions. The issue is not related to missing data or information, but rather how to use and apply that information in calibrating the transfer functions.

- Various design features for jointed plain concrete pavements (JPCP) were not adequately covered from the one LTPP section located in Wyoming. More importantly, WYDOT builds few rigid pavements that can be used in the calibration process.

Non-LTPP sites were also selected to include soils and site conditions excluded from the LTPP sites in Wyoming and adjacent states. The non-LTPP sites are discussed in the next section of this chapter.

2.2 Non-LTPP Test Sections

An additional 10 roadway segments were identified and included in the calibration process to represent more recent policies and practices being used by the Department (WYDOT, 2010). In addition, these sites were selected to include different soil types and layer thicknesses found in Wyoming. Nine of the sites were new flexible pavements and one was a new semi-rigid pavement. No additional rigid pavement segments were included because so few rigid pavements are built in Wyoming. Details on these sites are provided in a separate report (ARA, 2015).

2.3 Site Conditions and Design Features

The appropriate input parameters or values for each of the LTPP and non-LTPP segments were determined for each calibration site and used to confirm the applicability of the global default inputs values that were unavailable from WYDOT's construction files or the LTPP database.

2.3.1 *Field Investigations*

Field investigations for the LTPP sections were completed within the LTPP program and data from these field investigations are stored in the LTPP database. All data used in the calibration study for the LTPP segments was extracted from the LTPP database.

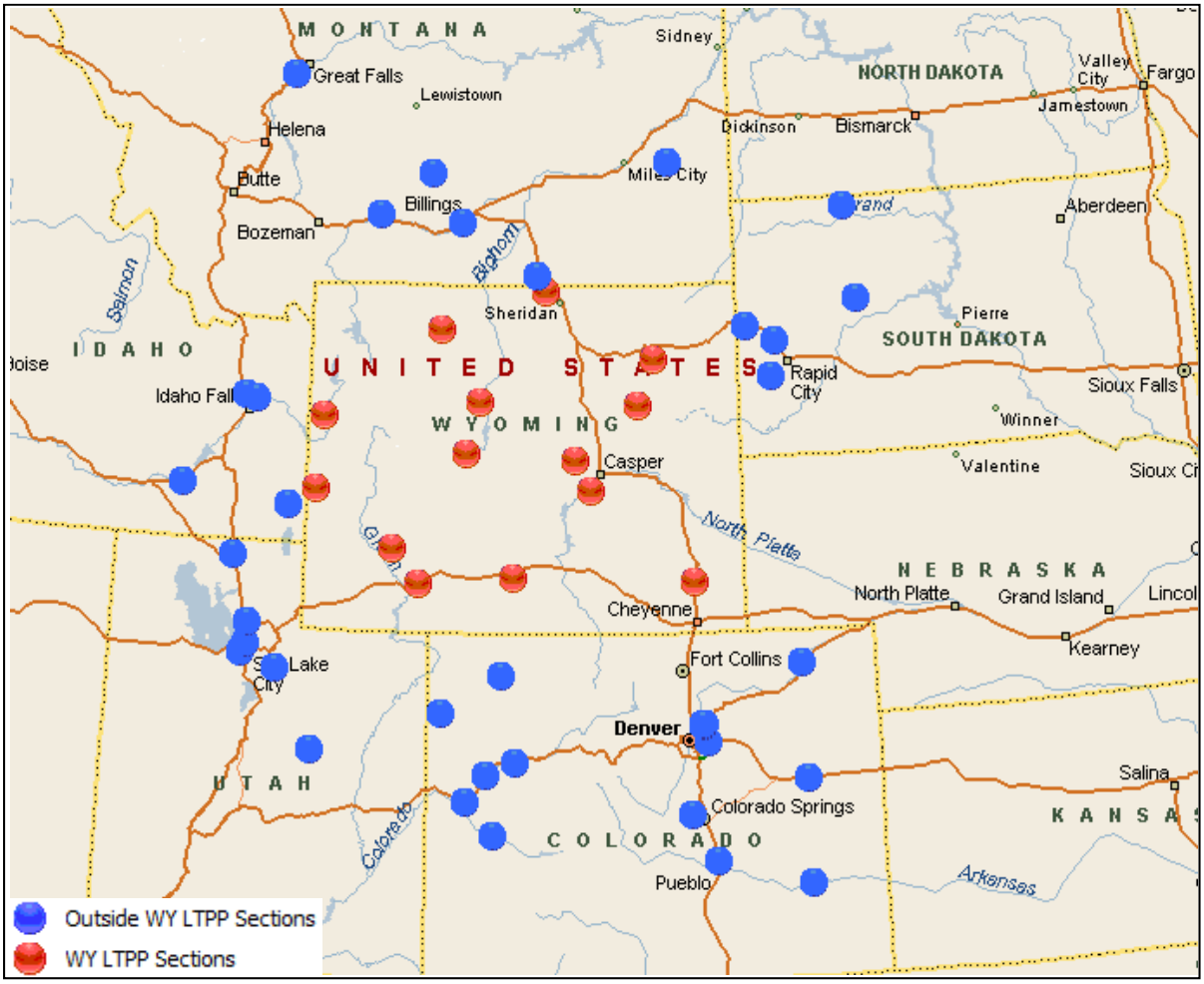

Figure 1—Location of LTPP Sites in Wyoming and Adjacent States

For the non-LTPP roadway segments, a field investigation was conducted by the University of Wyoming. The data from this project is documented in a separate report (ARA, 2015). The field investigations included condition surveys to determine the type and severity of pavement distress, a coring program for confirming and measuring layer thicknesses, and recovering materials for laboratory testing. The laboratory testing program included selected volumetric properties of the HMA layers.

2.3.2 *Climate/Weather Stations*

The MEPDG requires the location of a project be defined by its longitude, latitude, and elevation in order to develop project specific climate data. The climate specific data for each project was generated using the closest weather station. Typically, each weather station had 96 to 116 months of climate data.

Table 1—Number of LTPP Test Sections: Flexible or Semi-Rigid Pavements, New Construction and Rehabilitation

Flexible Pavement Type		Number of Test Sections With Full Time Series Data	
		Site ID	**Number**
New Construction	Flexible Pavement	8_0500[1]	4
		30_0100[1]	4
		56_1007, 56_6029, 56_6031, 56_6032, 56_7775,	26
		8_1029, 8_1047, 8_1053, 8_1057, 8_2008, 8_6013, 8_7780, 8_7781, 8_7783	
		16_1010, 16_1021, 16_6027,	
		30_6004, 30_7075, 30_7076, 30_7088, 30_8129	
		46_9106, 46_9187	
		49_1005, 49_1007	
	Semi-Rigid Pavement	56_2015, 56_2017, 56_2018, 56_2019, 56_2020, 56_2037, 56_7772, 56_7773	8
Rehabilitation	HMA Overlay of Flexible Pavement	8_0500[1]	11
		56_6029, 56_6031, 56_6032, 56_7775	17
		8_1029, 8_1047, 8_1053, 8_6002, 8_6013, 8_7780, 8_7781, 8_7783	
		30_6004, 30_7075, 30_7076, 30_7088, 30_8129	
	HMA Overlay of Semi-Rigid Pavement	56_2015, 56_2017, 56_2019, 56_2020, 56_7772	5
TOTAL		**68**	

NOTE:
1. Although there are multiple sections with performance data, these sections only represent one project.

2.3.3 Truck Traffic

Many of the truck traffic inputs for the Wyoming LTPP sections are at level 1 since volume and portable weigh-in-motion (WIM) data were available for many of the LTPP sites. The truck axle weight data were processed under a separate WIM study, and a detailed description of all traffic data for the LTPP WIM sites in Wyoming is presented within the WIM study report (ARA, 2012). All inputs used within the calibration study for the Wyoming sites were extracted from the traffic study and input values recommended for use. For the sites in adjacent states, the default values recommended for use in Wyoming were used, unless project specific data was available from the LTPP database, in which case those inputs were used for the calibration process.

Table 2—Number of LTPP Test Sections: Rigid Pavements, New Construction

Rigid Pavement Type		Number of Test Sections With Time Series Data						
		Site ID	Number	Dowel Diameter (in.)	Joint Spacing (feet)	Tied Shoulder	Slab Width (feet)	PCC-Base Contact Friction (months)
Jointed Plain Concrete Pavement (JPCP)	Granular	8_0213	12	1.25	15	Not tied	14	Full, entire design life
		8_0214		1.25	15	Not tied	12	
		8_0215		1.5	15	Not tied	12	
		8_0216		1.5	15	Not tied	14	
		8_0259		1.5	15	Tied	12	
		8_0811		1.25	15	Tied	12	
		8_0812		1.5	15	Tied	12	
		8_7776		1.25	14.5	Tied	12	
		46_3012		No dowels	15	Not tied	12	
		46_3013		No dowels	16	Not tied	12	
		46_3053		No dowels	15	Tied	12	
		56_3027		No dowels	15.75	Tied	12	
	Asphalt Treated Base (ATB)	8_0221	5	1.25	15	Not tied	14	Full, entire design life
		8_0222		1.25	15	Not tied	12	
		8_0223		1.5	15	Not tied	12	
		8_0224		1.5	15	Not tied	14	
		16_3017		1.25	16.9	Tied	14	
	Cement Treated Base (CTB)	8_0217	9	1.25	15	Not tied	14	Partial, 120 months
		8_0218		1.25	15	Not tied	12	
		8_0219		1.5	15	Not tied	12	
		8_0220		1.5	15	Not tied	14	
		8_3032		No dowels	17	Tied	12	
		49_3015		No dowels	12.5	Tied	12	
		49_7082		No dowels	12.5	Tied	12	
		49_7085		No dowels	12.5	Not tied	12	
		49_7086		No dowels	12.5	Not tied	12	
TOTAL SITES		**26**						

2.3.4 Layer/Material Properties

All of the input parameters for the different pavement layers were extracted from the LTPP database for the test sections located in Wyoming and in adjacent states. For the non-LTPP roadway segments, the layer thicknesses and other properties were measured during the field investigations or the recommended default values were used for the calibration process. As noted above the field investigations and data are documented and reported in a separate report that was completed by the University of Wyoming (ARA, 2015).

2.4 Summary of Verification-Calibration Test Sections

Table 3 summarizes the total number of sites for calibrating the distress transfer functions and smoothness regression equations. Restricting the number of sites to Wyoming would result in too few sections for the calibration process (18 conventional flexible pavements, 14 semi-rigid pavements, and 1 JPCP). Combining the LTPP sites in adjacent states with

similar design features results in a number of rigid sites that are considered borderline (26 sites), while the number of conventional flexible pavement sections are considered sufficient (86 sites) for determining the Wyoming calibration coefficients. The number of semi-rigid pavements (14 sites) is still considered too few to accurately derive the calibration coefficients.

Table 3—Number of Verification-Calibration Test Sections for Wyoming

Type of Roadway Segments		Flexible Pavement Sites	Semi-Rigid Pavement Sites	Rigid Pavement Sites (JPCP)
Wyoming Sections	LTPP	9	13	1
	Non-LTPP	9	1	0
Adjacent States	LTPP	68	0	25
	Non-LTPP	0	0	0
Total		86	14	26

As summarized in table 3, the verification-calibration sites used to derive the Wyoming transfer function calibration coefficients are located in adjacent states. Thus, the calibration coefficients for conventional flexible and rigid pavements are considered Rocky Mountain calibration coefficients.

CHAPTER 3 — CALIBRATION COEFFICIENTS FOR RIGID PAVEMENTS AND PCC OVERLAYS

Verification of the MEPDG global calibration coefficients and standard deviations of the rigid pavement transfer functions for Wyoming conditions consisted of running the *Pavement ME Design* software for the Wyoming LTPP and other LTPP JPCP sections located in adjacent states and evaluating goodness of fit and bias. The design features of the LTPP sections in adjacent states include a wide range of slab thickness (7.6 to 12.9 in.), transverse joint spacing (12.5 to 17 ft.), base types and subgrade soils. Most of the JPCP projects included dowel bars at transverse joints with dowel diameters ranging from 1.25 to 1.50 in. Table 4 lists the range of pavement features that were used for the verification-calibration process.

Table 4—Features and Characteristics of Rigid Pavement Structures Used for Calibration

Pavement Feature	Range	Mean or Typical Value
Age of JPCP	22 to 45 years	26 years
No. of Trucks (Design Lane)	0.48 to 26 million	14 million
Slab Thickness	7.6 to 12.9 inch	10 inch
Joint Spacing	12.5 to 17 feet	15 feet
Dowel Bars	None, 1.25 to 1.5 inch	1.25 inch
Base Type	Granular, ATB, CTB	ALL
Subgrade Type	A-6 to A-1-a	ALL

The AASHTO adopted global model or calibration coefficients utilized were those developed under NCHRP project 20-07 (327) to reflect corrections made to the concrete coefficient of thermal expansion (CTE) values (Sachs, 2014). The correct CTE values used in the NCHRP project 20-07 (327) were used in evaluating and judging the accuracy of the transfer functions for the rigid pavement test sections. Thus, proper lab measurements of CTE using AASHTO T336 *Coefficient of Thermal Expansion of Hydraulic Cement Concrete* can be directly input into the design of all PCC pavements and overlays.

This chapter discusses the verification and calibration of the distress transfer functions and International Roughness Index (IRI) regression equation for predicting the performance of JPCP in Wyoming.

3.1 JPCP Fatigue Cracking or Mid-Slab Cracking

3.1.1 Transfer Function

Two key models are used to predict mid-slab transverse fatigue cracking: (1) one model for determining the allowable number of loading cycles for a specific condition, and (2) a model for estimating the percentage of cracks slabs from the cumulative damage index. Equation 1 is used to estimate the fatigue life (N) of PCC slabs when subjected to repeated wheel load stresses and curling stresses (at both top and bottom of the slab) for a given flexural bending beam strength. The calibration factors C_1 and C_2 can be modified but since they are based on

substantial laboratory and full scale field testing data, the MEPDG Manual of Practice does not recommend changing these coefficients. These values are $C_1 = 1.0$ and $C_2 = -1.22$ which were held constant for the Wyoming calibration process.

$$\log\left(N_{i,j,k,l,m,n}\right) = C_1 \cdot \left(\frac{MR_i}{\sigma_{i,j,k,l,m,n}}\right)^{C_2} \quad (1)$$

The transfer function with appropriate model coefficients is the S-shaped curve giving the relationship between the measured fatigue cracking and accumulated fatigue damage (DF) at top and bottom of the JPCP slabs. Calibration coefficients C_4 and C_5 in equation 2 can be adjusted to remove bias and improve the goodness of fit with field data.

$$CRK = \frac{1}{1 + C_4\left(DI_F\right)^{C_5}} \quad (2)$$

Values derived for the global calibration coefficients are listed below and were obtained from NCHRP 20-07 (327) (Sachs, et al., 2014). These values were evaluated for adequacy against the measured Wyoming JPCP cracking data:

$C_4 = 0.52$
$C_5 = -2.17$

3.1.2 Verification of the Global Calibration Coefficients

Measured transverse cracking trends for all Wyoming calibration sections were evaluated for reasonableness. Whenever there was a significant time sequence aberration in the data, the individual cracking measurements were removed from the analysis when the data point was defined as an outlier.

Figure 2 presents a histogram of all measured (including time series) transverse cracking for the LTPP projects included in the analysis. The information provided in the figure shows a limited distribution of measured transverse cracking data, with most of the measured cracking being zero. Because the measured transverse cracking was mostly zero, commonly applied statistical procedures could not be used to evaluate goodness of fit and bias. The researchers thus applied non-statistical methods to verify the suitability of the MEPDG global transverse cracking model for local Wyoming conditions.

Verification of the MEPDG global JPCP transverse cracking model for Wyoming conditions consisted of the running the MEPDG analysis with the global transverse cracking model for all selected projects. For this analysis, the NCHRP Project 20-07(327) JPCP MEPDG global model coefficients were applied, since these coefficients are compatible with MDOT and LTPP revised PCC CTE data used in transverse cracking predictions. The outcomes of the analyses are presented in the following sections.

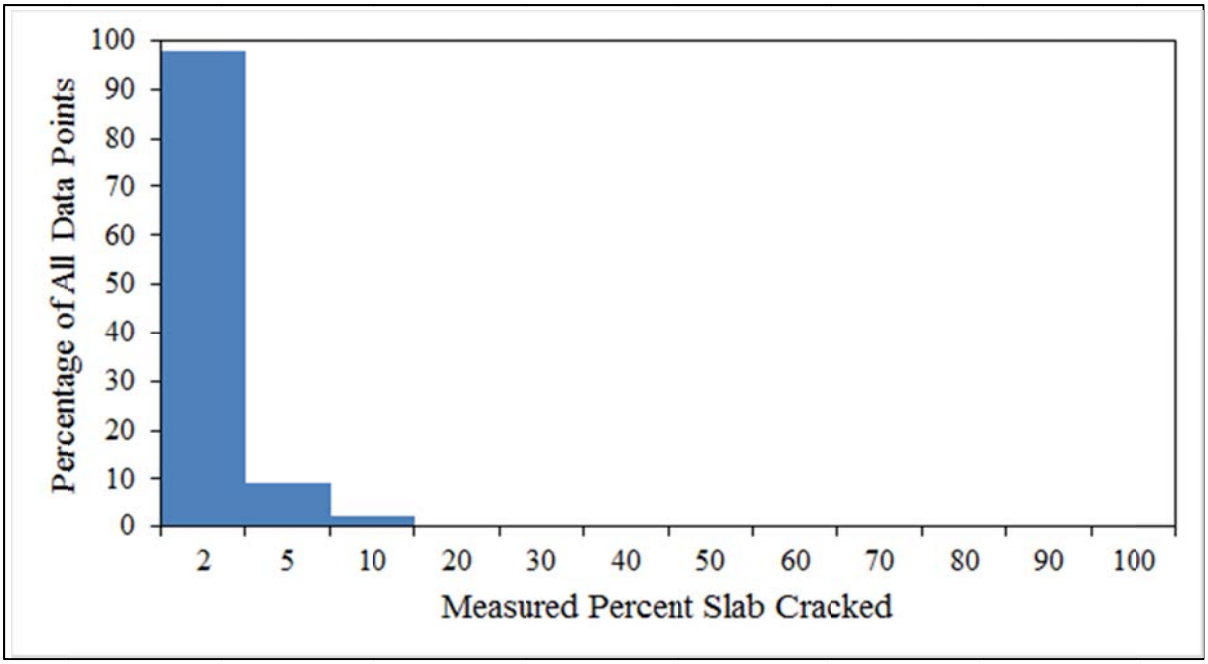

Figure 2—Histogram showing distribution of measured transverse slab cracking

3.1.3 Comparison of Measured and Predicted Transverse Faulting Groupings

For this comparison, transverse cracking was categorized into four groups, as shown in table 5. The goal was to determine how often measured and predicted transverse cracking fell in the same grouping. The range of each group was determined based on the distribution of the data available and using engineering judgment.

Table 5—Comparison of measured and predicted JPCP transverse slab cracking

Measured JPCP Transverse Cracking, percent slabs	**Predicted JPCP Transverse Cracking, percent slabs**		
	0-2	**2-5**	**>5**
0-2	142	0	0
2-5	13	0	0
>5	3	0	0

Total number of data points = 158

A review of the information presented in Table 5 showed the following:

- Approximately 90 percent of all data points (142 of 158) fell within the same measured and predicted transverse cracking grouping (0 to 2 percent cracking).
- Approximately 8 percent of the data points (13 of 158) fell within an adjacent grouping (i.e., measured grouping 2 to 5 against predicted grouping 0 to 2).
- For the remaining two percent of the data points (3 of 158) fell within an adjacent grouping (i.e., measured grouping >5 against predicted grouping 0 to 2).

The results show that a significant majority of predicted transverse cracking fell within the same grouping (over 90 percent), indicating that the global model predicted transverse cracks accurately with little bias.

The non-statistical procedures applied to determine goodness of fit and bias indicated that the MEPDG global transverse cracking model predicted transverse cracking reasonably well, with no significant bias in Wyoming. Therefore, there was no need for local calibration of the global transverse cracking model at this stage. However, the model should be evaluated in the future to determine how well it predicts significant levels of cracking (non-zero values). This can be done through continuous monitoring of the selected JPCP projects used in this analysis and/or adding non-LTPP JPCP sites that were built in Wyoming.

Figure 3 compares the predicted and measured percent slabs cracked, while figure 4 compares the calculated concrete fatigue damage index accumulated over time to the measured percent slabs cracked.

The fatigue cracking SEE derived from the Wyoming calibration sections was very low compared to the global standard deviation (0.083 percent slabs cracked versus 4.58 percent from NCHRP 20-07(327)). This outcome will significantly affect the design reliability prediction. A major limitation of this outcome, however, is the few number of actual projects included in the database and the fact that most of them had no cracking. Thus, it was decided to recommend use of the global standard deviation equation (standard error of the estimate [SEE]) shown below from NCHRP 20-07 (327):

$$\text{Standard Deviation (CRACK)} = 3.5522^{*} (\text{CRACK})^{0.3415} + 0.75 \qquad (3)$$

Where: CRACK = Predicted mean transverse cracking, percent

This standard deviation equation will provide a more realistic impact of design reliability on pavement design because it is based on hundreds of JPCP projects around the country. As more data on percent cracked slabs become available over time for these and other calibration sties, WYDOT should periodically verify and validate the Wyoming calibration coefficients and the standard error of the transfer function.

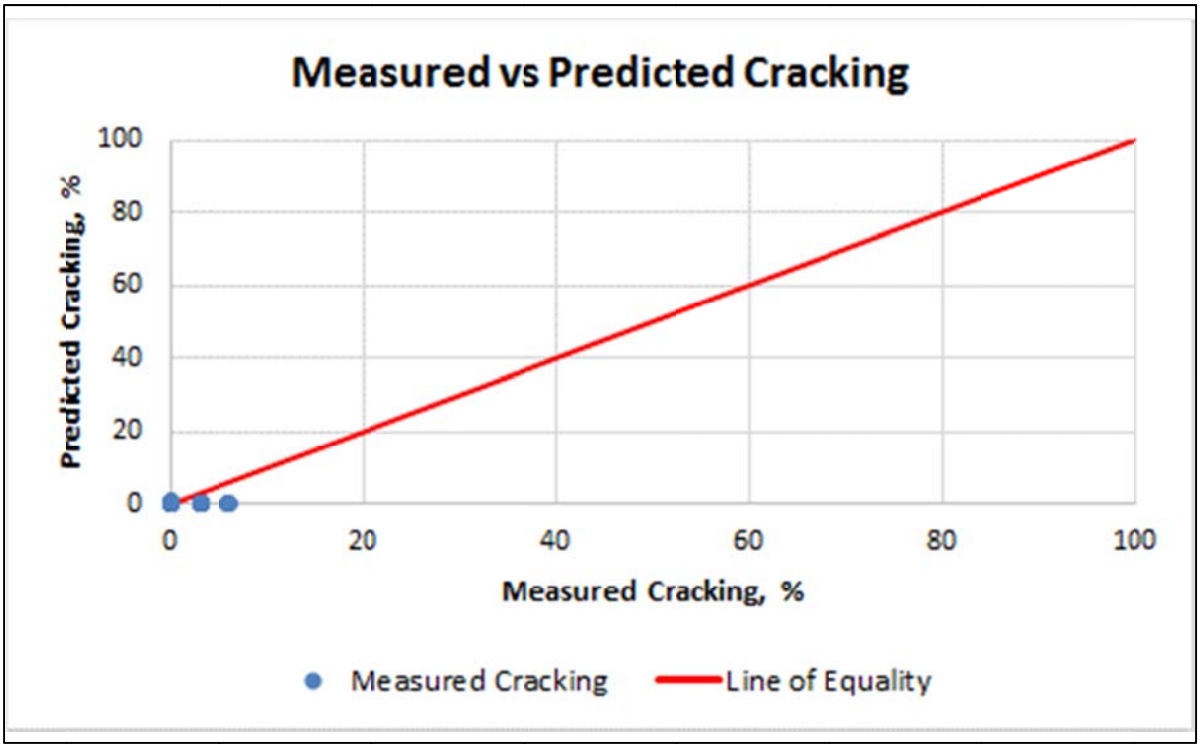

Figure 3—Predicted versus Measured Percent Slabs Cracked

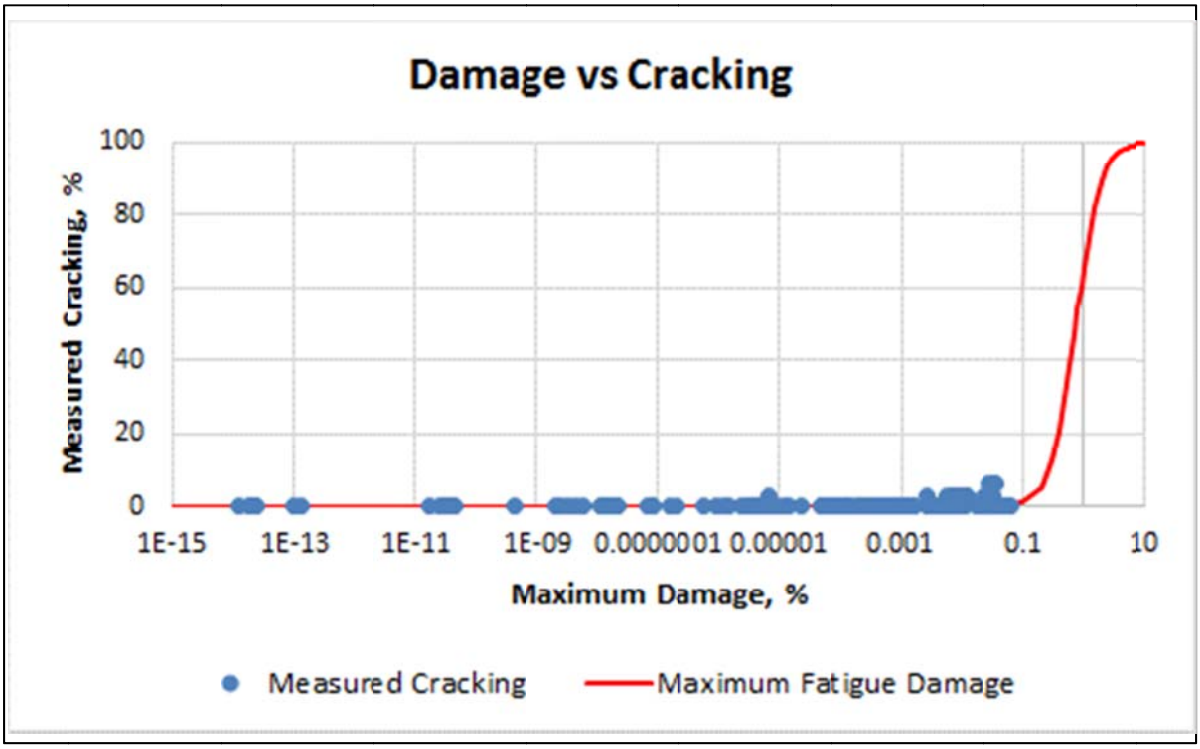

Figure 4—Measured Fatigue Transverse Cracking versus Concrete Fatigue Damage for all Wyoming and Neighboring States LTPP JPCP Sections

3.2 JPCP Faulting

3.2.1 Transfer Function

The mean transverse joint faulting is predicted using a complex incremental approach. A detailed description of the faulting prediction process is presented in Section 5 the MEPDG Manual of Practice. MEPDG faulting is predicted using the models presented below:

$$Fault_m = \sum_{i=1}^{m} \Delta Fault_i \tag{4}$$

$$\Delta Fault_i = C_{34} * (FAULTMAX_{i-1} - Fault_{i-1})^2 * DE_i \tag{5}$$

$$FAULTMAX_i = FAULTMAX_0 + C_7 * \sum_{j=1}^{m} DE_j * Log(1 + C_5 * 5.0^{EROD})^{C_6} \tag{6}$$

$$FAULTMAX_0 = C_{12} * \delta_{curling} * \left[Log(1 + C_5 * 5.0^{EROD}) * Log(\frac{P_{200} * WetDays}{p_s}) \right]^{C_6} \tag{7}$$

Where:

$Fault_m$ = Mean joint faulting at the end of month m, in.
$\Delta Fault_i$ = Incremental change (monthly) in mean transverse joint faulting during month *i*, in.
$FAULTMAX_i$ = Maximum mean transverse joint faulting for month *i*, in.
$FAULTMAX_0$ = Initial maximum mean transverse joint faulting, in.
$EROD$ = Base/subbase erodibility factor
DE_i = Differential deformation energy accumulated during month *i*. Computed using various inputs including joint LTE and dowel damage
$EROD$ = Base/subbase erodibility factor
$\delta_{curling}$ = Maximum mean monthly slab corner upward deflection PCC due to temperature curling and moisture warping.
P_S = Overburden on subgrade, lb.
P_{200} = Percent subgrade soil material passing No. 200 sieve
$WetDays$ = Average annual number of wet days (greater than 0.1 in. rainfall)

$$C_{12} = C_1 + C_2 * FR^{0.25} \tag{8}$$

$$C_{34} = C_3 + C_4 * FR^{0.25} \tag{9}$$

FR = Base freezing index defined as percentage of time the top base temperature is below freezing (32°F) temperature.

Dowel joint damage accumulated for the current month is determined from the following equation:

$$\Delta DOWDAM_{tot} = \sum_{j=1}^{N} C_8 * F_j \frac{n_j}{d f_c^*} \quad (10)$$

Where:

$\Delta DOWDAM_{tot}$ = Cumulative dowel damage for the current month.

n_i = Number of axle load applications for current increment and load group *j*.

N = Number of load categories.

f_c^* = PCC compressive stress estimated.

C_8 = Calibration constant.

F_j = Effective dowel shear force induced by axle loading of load category j.

C_1 through C_8 are calibration constants to be established based on field performance.

Faulting model calibration involved determination of the calibration parameters C_1 through C_7 from the above equations and the rate of dowel deterioration parameter, C_8, from the above equation, which minimize the error function, ERR, defined as:

$$ERR(C_1, C_2, ..., C_8) = \sum_{ob=1}^{Nob} \left(FaultPredicted_{ob} - FaultMeasured_{ob}\right)^2 \quad (11)$$

Where:

ERR = Error function

$C_1, C_2, ..., C_8$ = Calibration parameters

$FaultPredicted_{ob}$ = Predicted faulting for observation *ob* in the calibration database

$FaultMeasured_{ob}$ = Measured faulting for observation *ob* in the calibration database

N_{ob} = Number of observation in the calibration database

The global calibration coefficients from NCHRP 20-07(327) are as follows (Sachs, 2014):

C1 = 0.595
C2 = 1.636
C3 = 0.00217
C4 = 0.00444
C5 = 250
C6 = 0.47
C7 = 7.30
C8 = 400

The global faulting model for standard deviation as a function of mean joint faulting is given in equation 12.

$$\text{Standard Deviation (FAULT)} = 0.07162 * (\text{FAULT})^{0.368} + 0.00806 \quad (12)$$

Where: FAULT = Predicted mean joint faulting, in.

3.2.2 Verification of the Global Calibration Coefficients

Only data from the Wyoming and neighboring states LTPP sections were available for use on this project. Measured faulting trends for each section were carefully reviewed. There existed some significant variations over time for nearly all sections probably due to variable curling of the slabs. Whenever there was a significant time sequence aberration in the data, the individual faulting measurements were removed from the analysis; similar to what was done for the JPCP fatigue cracking data.

Figure 5 shows the predicted versus measured faulting using the global calibration coefficients for all data. The plot shows poor goodness of fit along with an obvious bias of over predicted faulting. However, the magnitude of faulting is generally low with the highest values just exceeding the threshold value normally used in design. The reason for the low faulting values is the stabilization of the base and the standard practice by WYDOT and neighboring states to use dowels on many JPCP projects.

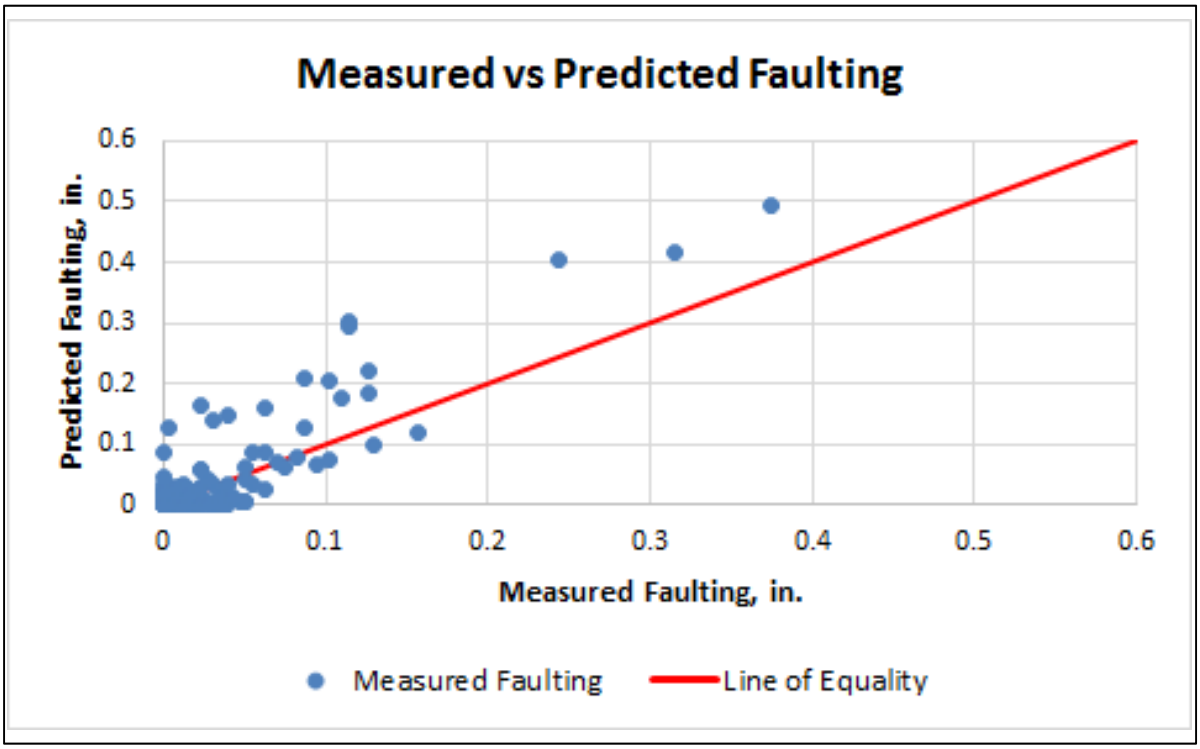

Figure 5—Predicted versus Measured Faulting using NCHRP 20-07(327) Global Calibration Coefficients

The predicted faulting versus the residual faulting error (predicted minus measured value) is included in figure 6 and shows a trend that confirms bias in the model. The magnitude of faulting, however, is very low. In fact, the magnitude is significantly lower than the threshold value normally used in design. The reason for low faulting values is that WYDOT and neighboring states have been doweling JPCP since the 1970's.

Table 6 includes results from the statistical analysis performed in comparing the predicted and measured faulting values. Results from the statistical analysis are summarized below:

- The intercept of the y= x curve was -0.00265 (ranging from -0.0068 to 0.0015) with a corresponding p-value of 0.2093. The p-value greater than 0.05 implied the Test 1 null hypothesis is accepted. Thus, the MEPDG faulting transfer function does not exhibit bias.

- The slope of the y= x curve was 1.35468 (ranging from 1.27452 to 1.43484) with a corresponding p-value of <0.0001. Thus, the test 2 null hypothesis was rejected, indicating the predicted MEPDG faulting is unequal to the measured faulting, and is significant. MEPDG faulting estimates cannot be extrapolated beyond or outside of the key inputs used for calibration.

- Finally, the p-value from the paired t-test comparing faulting estimated with the MEPDG to the measured faulting was 0.0288, which is less than 0.05. This shows that this aspect of bias was significant.

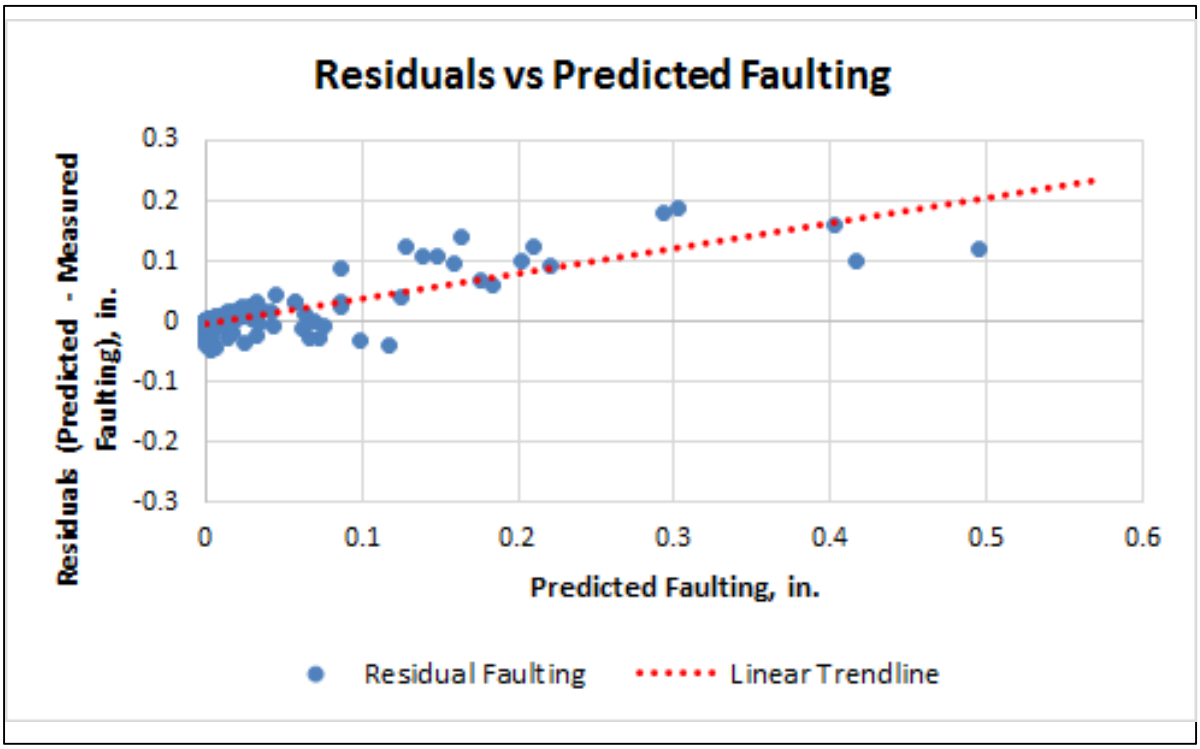

Figure 6—Residuals (Predicted minus Measured Value) versus Predicted for Faulting

Table 6—Statistical Comparison of Measured and MEPDG Predicted Faulting for Global Calibration Coefficients

Hypothesis Testing and T-Test				Goodness of Fit		
Test Type	**Value**	**Range**	**p-value**	**R^2**	**SEE, in.**	**N**
Hypothesis Test (1): Intercept = 0	-0.00265	-0.0068 to 0.0015	0.2093	0.7974	0.02975	242
Hypothesis Test (2): Slope = 1	1.35468	1.27452 to 1.43484	<0.0001			
Paired t-test	-	-	0.0288			

There are no obvious causes for over prediction of faulting using the NCHRP 20-07 (327) global faulting model coefficients for Wyoming. Thus, the global calibration coefficients are inappropriate for Wyoming conditions and design features, and local calibration is needed to adjust the model coefficients to match the measured transverse joint faulting data.

3.2.3 Wyoming Calibration Coefficients

The measured faulting trends for all calibration sections were evaluated for reasonableness. Most of the faulting time series data exhibited reasonable trends. As such, adjustments were made to the global calibrations coefficients to account for this difference or bias between the measured and predicted values. Local calibration was performed using these data, and the final set of Wyoming specific local joint faulting model coefficients are summarized below:

C1 = 0.5104
C2 = 0.00838
C3 = 0.00147
C4 = 0.08345
C5 = 5999
C6 = 0.504
C7 = 5.9293
C8 = 400

The standard deviation of the transverse joint faulting equation is shown in equation 13. The Wyoming standard deviation equation is similar to the globally derived model and is believed to provide a reasonable assessment of variation for joint faulting prediction.

$$\text{Standard Deviation (FAULT)} = 0.0831 * (\text{FAULT})^{0.3426} + 0.00521 \qquad (13)$$

Where: FAULT = Predicted mean joint faulting, in.

Figure 7 shows the predicted versus measured faulting using the Wyoming local calibration coefficients. The plot shows reasonable goodness of fit ($R^2 = 0.60$ and SEE = 0.03 in.) along with no obvious bias of under or over prediction of faulting.

One limitation of the calibration is that there are only a few sections with measured transverse joint faulting above 0.12 in. and the maximum was 0.15 in. Typical design criteria range from 0.10 to 0.20 in. and it would be better if there were more JPCP sections that exhibit higher faulting to provide better validation. However, the faulting prediction model does predict reasonably well up to the 0.15 in. When properly sized dowel bars are used the amount of joint faulting is typically very low as shown by these data.

Table 7 summarizes the statistical validation analysis between the predicted and measured faulting data for the JPCP pavement sections. The outcome of the three statistical tests to validate that the prediction models for the faulting transfer function is not biased:

- The intercept of the y= x curve was 0.00055 (95 percent confidence interval ranges from -0.00217 to 0.00328) which includes the null hypothesis of 0.00 with a

corresponding p-value of 0.6902. The p-value greater than 0.05 means the null hypothesis that the intercept is zero is accepted. Thus, the predicted versus measured faulting line did not exhibit bias related to the intercept.

- The slope of the y= x curve was 1.00638 which is equal to the null hypothesis slope of 1.00. The 95 percent confidence interval ranges from 0.95388 to 1.05889 which includes 1.00 with a corresponding p-value of 0.8109. The p-value greater than 0.05 means the null hypothesis was accepted, indicating that the slope between predicted and measured faulting is close to 1.00 indicating no bias.

- Finally, a direct comparison of measured and predicted faulting for each section was made across the entire database using the paired t-test. The p-value from paired t-testing was 0.6435 value (>0.05) and thus the null hypothesis (that the mean difference between predicted and measured cracking across all observations are equal) was accepted. This indicates no bias related to predicted and measured values over the entire database.

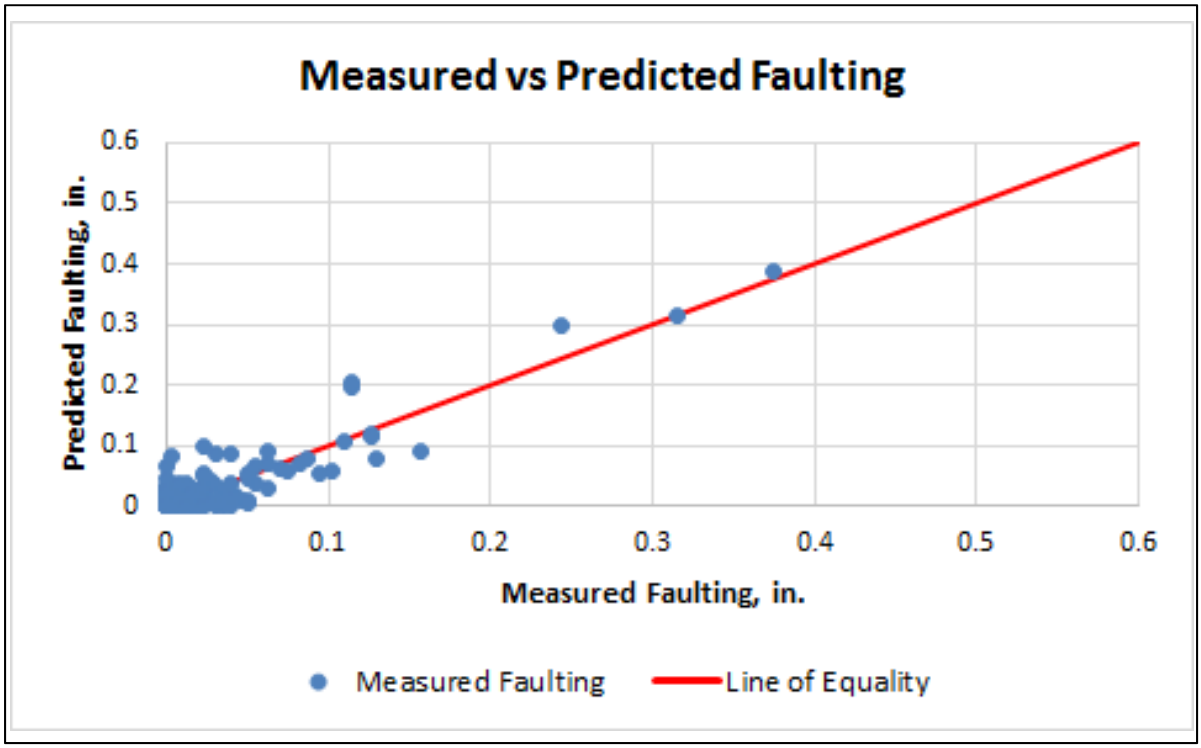

Figure 7—Predicted versus Measured Joint Faulting using Wyoming JPCP Calibration Coefficients

These results suggest that the Wyoming calibrated joint faulting transfer function and prediction methodology is not biased in over or under predicting faulting on average over the entire database. It is recommended that the Wyoming faulting transfer function be used for design of JPCP.

Table 7—Statistical Comparison of Measured and MEPDG Predicted Faulting for WYDOT Calibration Coefficients

Hypothesis Testing and T-Test				Goodness of Fit		
Test Type	**Value**	**Range**	**p-value**	**R^2**	**SEE, in.**	**N**
Hypothesis Test (1): Intercept = 0	0.00055	-0.00217 to 0.00328	0.6902	0.8281	0.01955	242
Hypothesis Test (2): Slope = 1	1.00638	0.95388 to 1.05889	0.8109			
Paired t-test	-	-	0.6435			

3.3 JPCP IRI or Smoothness

3.3.1 IRI Regression Equation

IRI is predicted for JPCP using the following regression equation:

$$IRI = IRI_I + J1*CRK + J2*SPALL + J3*FAULT + J4*SF \quad (14)$$

Where:

IRI_I = Initial IRI after construction, in./mile
CRK = JPCP transverse fatigue cracking, percent slabs
$SPALL$ = JPCP joint spalling, percent joints
$FAULT$ = JPCP mean joint faulting, mean of all joints in inches
SF = Site factor (includes subgrade fine content, freezing index, age)
$J1, J2, J3, J4$ = Global calibration coefficients (J1 = 0.8203, J2 = 0.4417, J3 = 1.4929, J4 = 25.24)

3.3.2 Verification of Global Calibration Coefficients

A plot of predicted and measured IRI for the Wyoming LTPP sites is shown in figure 8, as well as the R-Squared, SEE, and number of observations. These results indicate that goodness of fit was reasonable and the model predictions appear to be unbiased with Wyoming data. The SEE for the global regression equation of 10.2 in./mile. The predicted IRI versus the residual IRI error (predicted minus measured value) is included in figure 9 and shows no trend that confirms no bias in the model.

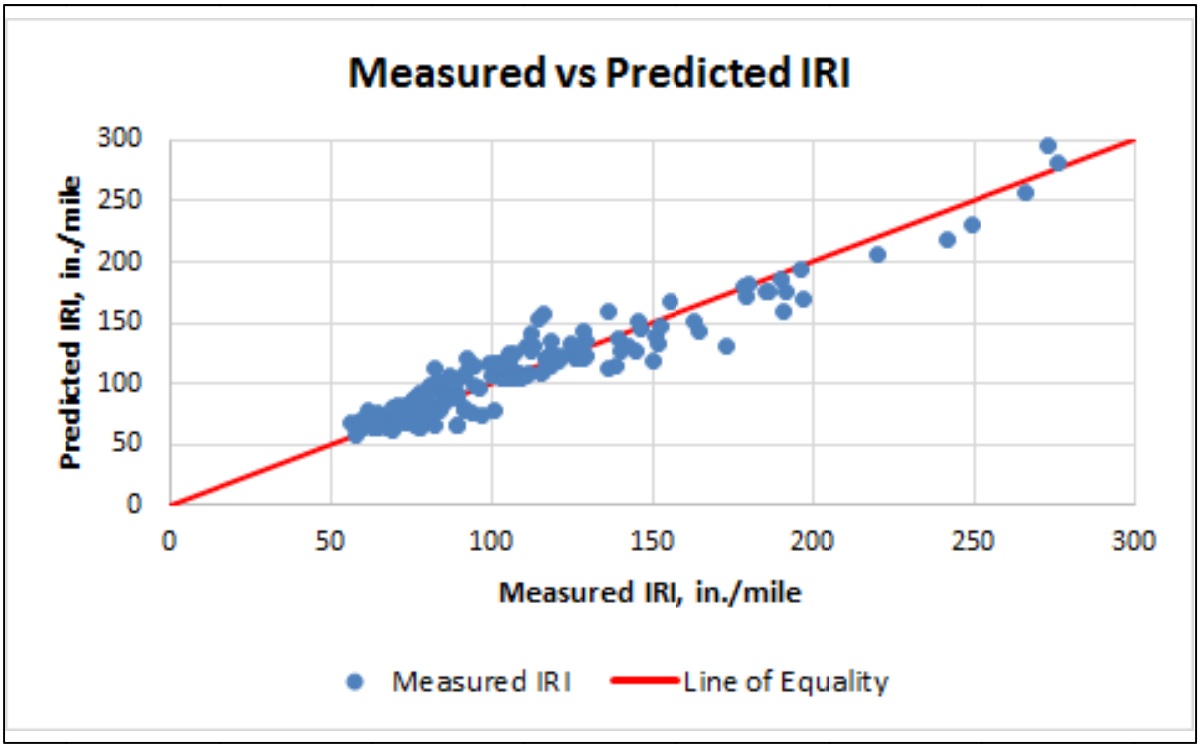

Figure 8—Predicted versus Measured IRI for Wyoming LTPP Sections using Global Calibration Coefficients

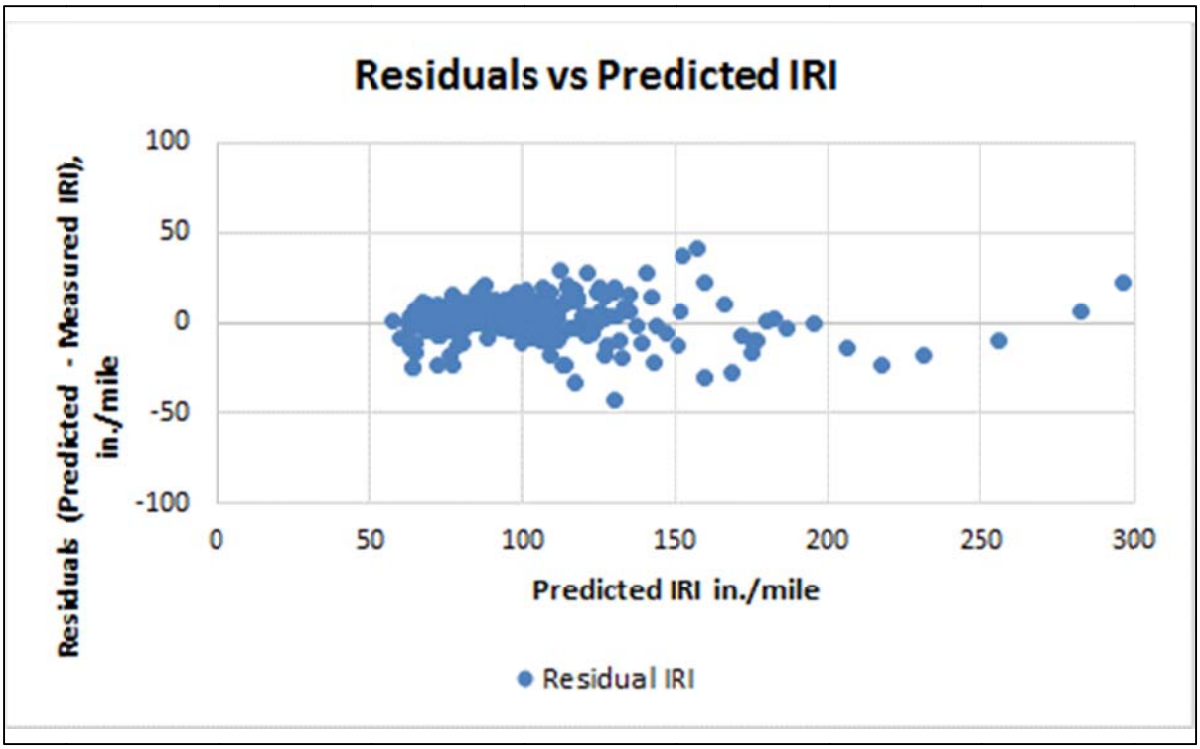

Figure 9—Residuals (Predicted minus Measured Values) versus Predicted for IRI

Table 8 summarizes the statistical analysis performed for comparing predicted and measured IRI values. The results are summarized as follows:

- The intercept of the y= x curve was 12.4 (ranging from 8.7 to 16) with a corresponding p-value of <0.0001. The p-value less than 0.05 implied the test 1 null hypothesis was rejected. Thus, the intercept exhibits bias. Since the IRI predictions are typically far above the intercept value of 12.4 in./mile, this bias is not considered as critical.

- The slope of the y= x curve was 0.99777. The 95 percent confidence interval was 0.98654 to 1.009 which includes the null hypothesis of 1.00. The corresponding p-value was 0.6967 which is greater than 0.05. Thus, the null hypothesis is accepted, indicating no bias of the IRI slope.

- Finally, the p-value from the paired t-test comparison of predicted IRI and measured IRI. The t-test p-value was 0.1112, thus, the null hypothesis is accepted indicating no bias.

The WYDOT IRI regression equation predicted IRI fairly close to the measured IRI values for most of the calibration sections.

Table 8—Statistical Comparison of Measured and Predicted IRI for Global Calibration Coefficients

Hypothesis Testing and T-Test				**Goodness of Fit**		
Test Type	**Value**	**Range**	**p-value**	**R^2**	**SEE, in./mile**	**N**
Hypothesis Test (1): Intercept = 0	12.4	8.7 to 16	<0.0001	0.8992	10.2	307
Hypothesis Test (2): Slope = 1	0.99777	0.98654 to 1.009	0.6967			
Paired t-test	-	-	0.1112			

Note that JPCP IRI standard error is estimated internally by the MEPDG.

CHAPTER 4 — CALIBRATION COEFFICIENTS FOR FLEXIBLE PAVEMENTS

Adjustment of the calibration coefficients and standard deviation equations of the flexible and semi-rigid pavement transfer functions for Wyoming conditions was completed in accordance with the AASHTO MEPDG Local calibration Guide (AASHTO, 2010). As noted in chapter 1, this procedure is a four-part process divided into multiple steps. The four major parts of the process included:

1. Determining the inputs for the for 32 LTPP and non-LTPP flexible and semi-rigid pavement test sections located in Wyoming, and the 68 LTPP flexible and semi-rigid pavement sections located in adjacent states (see table 3).
2. Verify the global calibration coefficients for each transfer function by executing the *Pavement ME Design*® software using the global calibration coefficients for the LTPP and non-LTPP sections and evaluating goodness-of-fit and bias for flexible and semi-rigid pavement test sections.
3. If significant bias is found, modify or adjust the coefficients of the transfer function to eliminate any bias and reduce the SEE or standard deviation between the predicted and measured values. In addition, determine whether the adjustment to the coefficients is dependent on some design feature or material/layer property.
4. Verify the resulting local calibration coefficients for each transfer function by executing the *Pavement ME Design*® software using the local or adjusted global calibration coefficients for the LTPP and non-LTPP sections and evaluate the goodness-of-fit and bias for the flexible and semi-rigid pavement test sections.

In summary, the predicted values are compared to the observed or measured values over time to determine if the transfer function exhibits significant bias and poor precision or high SEE values. The AASHTO MEPDG Local Calibration Guide (AASHTO, 2010) recommends both the intercept and slope of the relationship between the predicted and measured values be used to evaluate the null hypothesis (slope = 1 and intercept = 0). If the hypothesis is rejected for either test (the intercept or slope), the results from the confirmation runs are used with additional calibration sites to revise the coefficients of the distress transfer functions.

For the Wyoming LTPP and non-LTPP sections, too few were available by themselves for the verification and calibration process, so all Wyoming sections and the LTPP sections in adjacent states were used to verify and adjust the calibration coefficients (see chapter 2). The inclusion of all sections for verification and calibration represents a deviation from the procedure recommended for use in the AAHSTO MEPDG Local Calibration Guide.

The remainder of this chapter provides more detailed discussion on the results from the verification and local calibration of the transfer function coefficients for each distress predicted by the *Pavement ME Design*® software. Section 5 of the MEPDG Manual of Practice provides a review of all transfer functions and models that are used to predict distress and smoothness of flexible and semi-rigid pavements.

4.1 Rut Depth

4.1.1 Transfer Function

Two transfer functions are used to predict the total rut depth of flexible and semi-rigid pavements and hot mix asphalt (HMA) overlays: one for the HMA layers and the other one for all unbound aggregate base layers and subgrades. Both are presented within this subsection.

Hot Mix Asphalt Mixtures/Layers

The HMA calibrated transfer function was based on laboratory repeated load plastic deformation tests and is shown below.

$$\Delta_{p(HMA)} = \varepsilon_{p(HMA)} h_{HMA} = \beta_{1r} k_z \varepsilon_{r(HMA)} 10^{k_{1r}} n^{k_{2r}\beta_{2r}} T^{k_{3r}\beta_{3r}} \quad (15)$$

Where:

$\Delta_{p(HMA)}$ = Accumulated permanent or plastic vertical deformation in the HMA layer/sublayer, in.
$\varepsilon_{p(HMA)}$ = Accumulated permanent or plastic axial strain in the HMA layer/sublayer, in./in.
$\varepsilon_{r(HMA)}$ = Resilient or elastic strain calculated by the structural response model at the mid-depth of each HMA sublayer, in./in.
$h_{(HMA)}$ = Thickness of the HMA layer/sublayer, in.
n = Number of axle load repetitions.
T = Mix or pavement temperature, °F.
k_z = Depth confinement factor.
$k_{1r,2r,3r}$ = Global field calibration parameters (from the NCHRP 1-40D recalibration; k_{1r} = -3.35412, k_{2r} = 0.4791, k_{3r} = 1.5606).
β_{1r}, β_{2r}, β_{3r}, = Local or mixture field calibration constants; for the global calibration, these constants were all set to 1.0.

$$k_z = (C_1 + C_2 D)0.328196^D \quad (16)$$

$$C_1 = -0.1039(H_{HMA})^2 + 2.4868 H_{HMA} - 17.342 \quad (17)$$

$$C_2 = 0.0172(H_{HMA})^2 - 1.7331 H_{HMA} + 27.428 \quad (18)$$

D = Depth below the surface, in.
H_{HMA} = Total HMA thickness, in.

Unbound Granular Aggregate Base Layer and Subgrade Soils

Equation 19 shows the rut depth transfer function for the unbound layers and subgrade.

$$\Delta_{p(soil)} = \beta_{s1} k_{s1} \varepsilon_v h_{soil} \left(\frac{\varepsilon_o}{\varepsilon_r} \right) e^{-\left(\frac{\rho}{n}\right)^{\beta}} \quad (19)$$

Where:

$\Delta_{p(Soil)}$ = Permanent or plastic deformation for the layer/sublayer, in.
n = Number of axle load applications.

ε_o = Intercept determined from laboratory repeated load permanent deformation tests, in./in.
ε_r = Resilient strain imposed in laboratory test to obtain material properties ε_o, β, and ρ, in./in.
ε_v = Average vertical resilient or elastic strain in the layer/sublayer and calculated by the structural response model, in./in.
h_{Soil} = Thickness of the unbound layer/sublayer, in.
k_{s1} = Global calibration coefficients; k_{s1}=2.03 for granular materials and 1.35 for fine-grained materials.
β_{s1} = Local calibration constant for the rutting in the unbound layers; the local calibration constant was set to 1.0 for the global calibration effort.

$$Log\beta = -0.61119 - 0.017638(W_c) \quad (20)$$

$$\rho = 10^9 \left(\frac{C_o}{\left(1 - \left(10^9\right)^\beta\right)} \right)^{\frac{1}{\beta}} \quad (21)$$

$$C_o = Ln\left(\frac{a_1 M_r^{b_1}}{a_9 M_r^{b_9}} \right) = 0.0075 \quad (22)$$

W_c = Water content, percent.
M_r = Resilient modulus of the unbound layer or sublayer, psi.
$a_{1,9}$ = Regression constants; a_1=0.15 and a_9=20.0.
$b_{1,9}$ = Regression constants; b_1=0.0 and b_9=0.0.

4.1.2 Verification of Global Calibration Coefficients

The rut depths for all flexible and semi-rigid pavements were calculated with *Pavement ME Design*®. Figure 10 shows a comparison of the measured versus predicted total rut depths using the global calibration coefficients for all test sections in Wyoming and in adjacent states. As shown, there is a bias in the predicted rut depths and the goodness-of-fit is considered poor. The MEPDG over predicts the total rut depth, which has been found by many other agencies (Darter et al., 2009 and 2014; Mallela et al., 2013; Von Quintus and Moulthrop, 2007). Figure 11 shows the rut depths measured over time for the Wyoming sections and LTPP sections located in adjacent states. Two observations from this comparison are:

1. Some of LTPP sections located in adjacent states have been in service much longer than the Wyoming sections.
2. The measured rut depths are generally within the same range between the Wyoming and other agency data, but more of the LTPP sections in the adjacent states have exhibited higher rut depths. The higher rut depths, however, are not considered an anomaly relative to the Wyoming data.

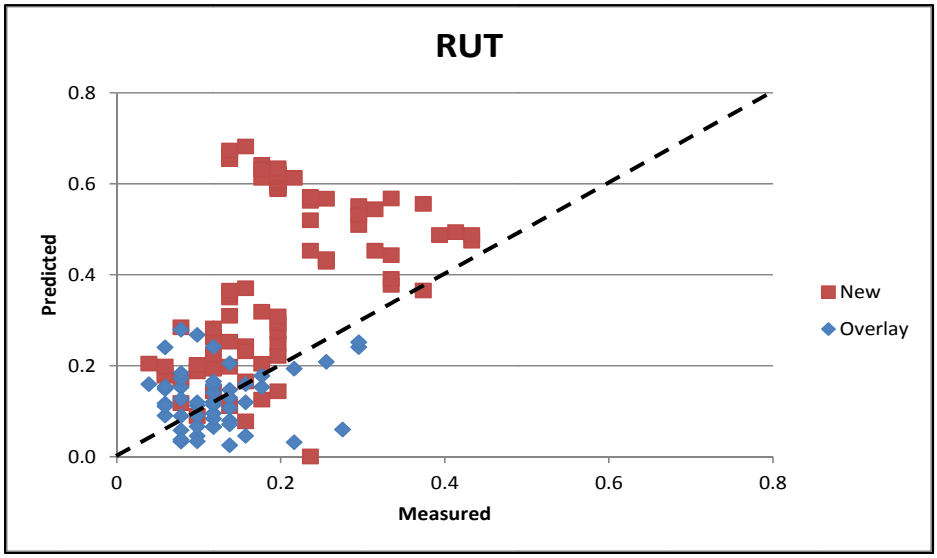

Figure 10—Predicted versus Measured Rut Depths using the Global Calibration Coefficients

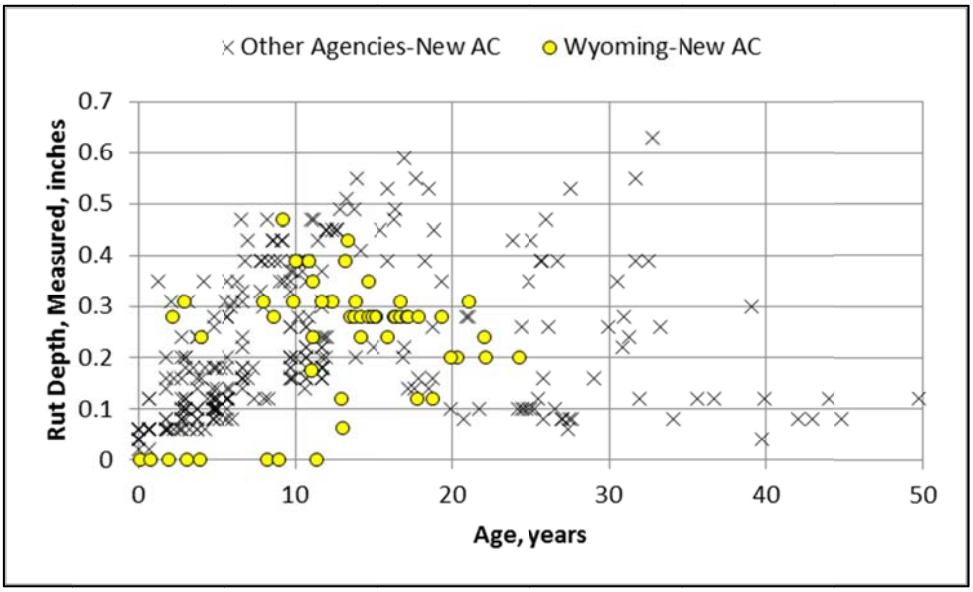

Figure 11—Rut Depths Measured with Time for the Section Located in Wyoming and in Adjacent States

Figure 12 shows the measured and predicted rut depths for just the Wyoming sections. Use of the global calibration coefficients results in a similar observation; the MEPDG over predicts the total rut depth. The next step in the verification-calibration process was to determine if there are design features or other factors that impact the measured rut depths. Figure 13 shows the rut depths measured over time for the new flexible sections, semi-rigid sections, and HMA overlaid sections. Some important observations from this evaluation are:

- The HMA overlaid sections exhibit lower rut depths than for the new flexible and semi-rigid pavement sections.
- The non-LTPP sections exhibit a lot less rutting than the LTPP sections, which has also been observed by other agencies that have conducted a local calibration study (Darter, et al., 2009 and 2014; Von Quintus, et al., 2015). The reason for the lower rut depths for the Wyoming non-LTPP sections in comparison to the LTPP sections is unknown. In the other studies, it found that the measurement technique resulted in a bias between the LTPP and non-LTPP sections. The bias of the non-LTPP sections were adjusted through a multiplication factor so the bias or difference between the measurements was eliminated. There are too few non-LTPP sections to conclude the bias between the LTPP and non-LTPP sections is independent on some mixture property or specification. Thus, no adjustment was made to the rut depths of the non-LTPP test sections.
- The semi-rigid sections exhibit a wide range of rut depths measured over time, in that there appears to be two data sets of measured rut depths (see figure 13). An evaluation of the measured rut depths was completed to determine if a design feature could be used to explain the difference between the two sets of data. As an example, figure 14 shows the data sets segregated by HMA thickness above the cement stabilized layer. As shown, HMA thickness does not explain the difference in the rut depths measured over time. However, all of the semi-rigid sections with the higher rut depths have thicker HMA layers. The other parameter that can explain the higher rut depths measured for the thicker HMA layers is a loss of bond between the HMA layer and cement treated base layer. Layer bond is not recorded in the LTPP database, but would result in higher predicted rut depths that could explain this difference in measured values.

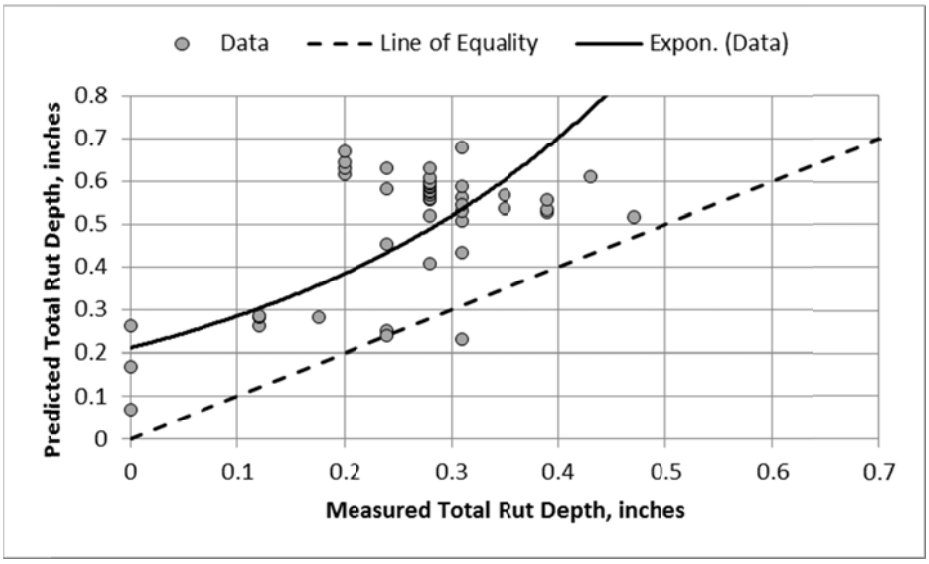

Figure 12—Predicted versus Measured Rut Depths using the Global Calibration Coefficients for the Wyoming LTPP and Non-LTPP Sections

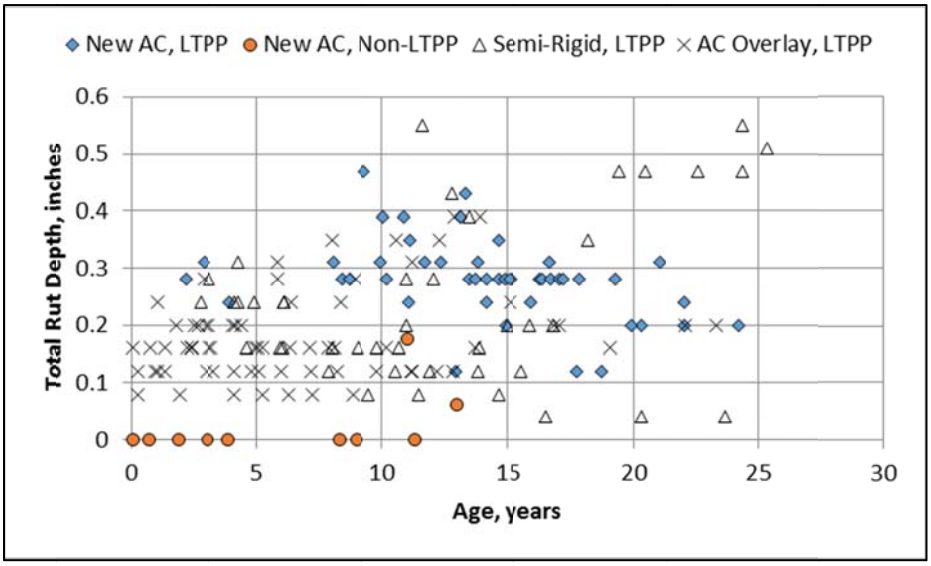

Figure 13—Rut Depths Measured with Time for the Wyoming LTPP and Non-LTPP Sections

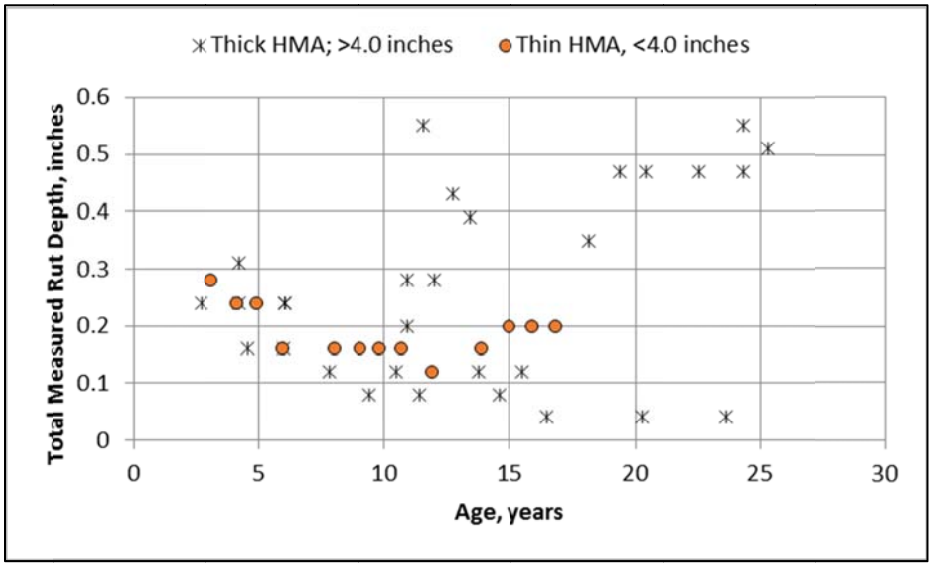

Figure 14—Rut Depths Measured with Time and Segregated by HMA Layer Thickness for the Wyoming LTPP and Non-LTPP Semi-Rigid Pavement Sections

During the analysis of the measured rut depth, an important observation was made regarding some of the LTPP sections. Many of the LTPP test sections exhibit irrational trends in the measured total rut depths with time or age. Figure 15 shows examples of the decrease in rut depths measured over time for some of the LTPP test sections. In summary, over 50 percent of the LTPP test sections, excluding the overlaid sections, exhibit this trend which cannot be predicted or explained by any mechanistic-empirical model.

The following lists some of the findings from the comparison of the predicted and measured rut depths (see figures 10 and 12).

- The slope between the measured and predicted total rut depths is significantly different from 1.0.
- The intercept is also significantly different from 1.0.

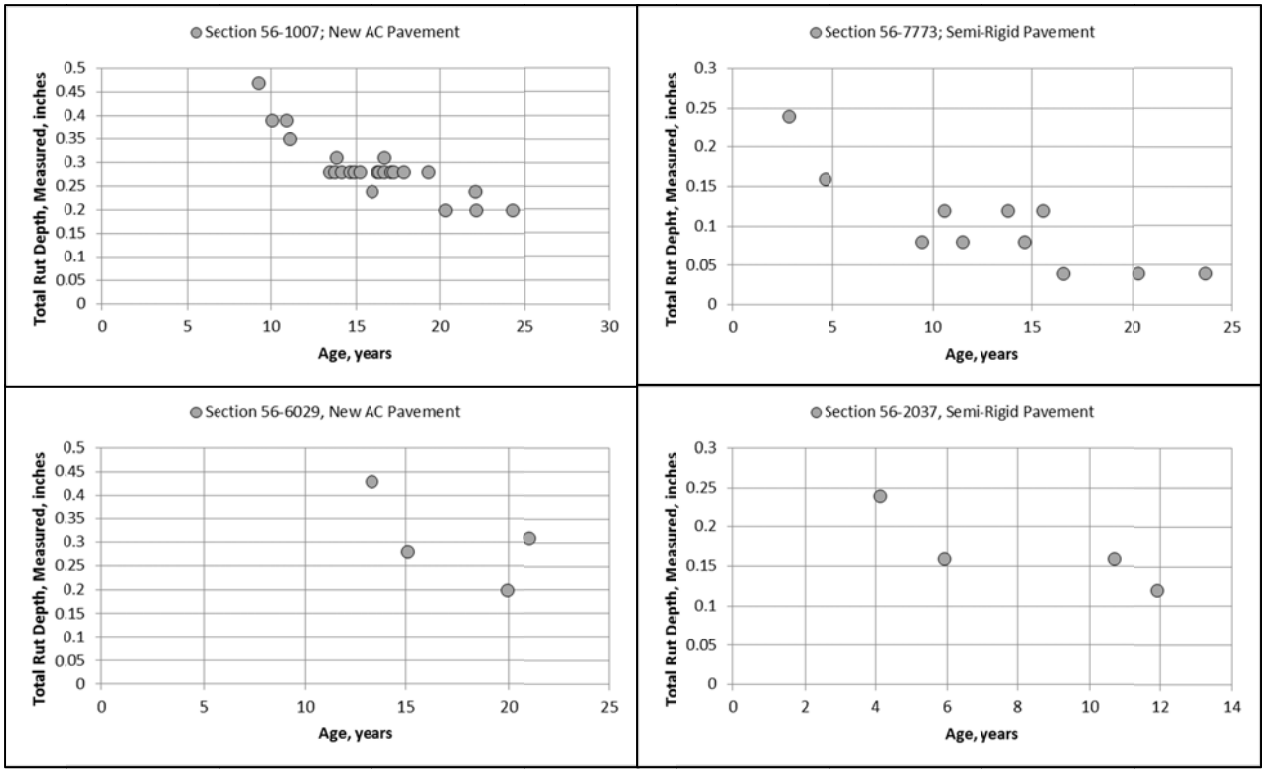

Figure 15— Some LTPP Sections that Exhibit Irrational Trends of Rut Depth

4.1.3 Wyoming Calibration Coefficients

As noted above, measured rut depth trends for each calibration section were carefully reviewed. Some significant variations or irrational results were observed for more than just a few sections. Thus, the analysis utilized the full Wyoming flexible pavement database to establish the goodness of fit and bias in the MEPDG rut depth transfer functions for the HMA and unbound layers.

The transfer function coefficients recommended for use from NCHRP project 9-30A were used as a starting point in deriving the Wyoming calibration coefficients for both the HMA and unbound layers (Von Quintus, et al., 2012). The steps used to determine the adjustments to the global calibration coefficients for the rut depth transfer functions are listed below:

- The HMA overlay sections and the semi-rigid pavements were initially used to derive the HMA calibration coefficients that minimize the bias between the predicted and measured rut depths. It was assumed that the rut depth or permanent deformation in the underlying unbound layers is minimal to nil for these structures.
- The conventional flexible pavement sections were used to derive the calibration coefficients for the unbound layers using the transfer function coefficients for the HMA layer that were estimated from the above step.
- All sections were then combined to eliminate any bias for the total rut depth.

The following summarizes the Wyoming calibration coefficients from this analysis.

- Calibration coefficients for all HMA mixtures:
  - K_1 = -2.45; this coefficient has been found to be related to the type of HMA mixtures in terms of polymer modified, but there are simply too few to separate out any impact for the sections in Wyoming.
  - K_2 = 0.30; this parameter is probably related to mixture type, but laboratory repeated load plastic deformation tests are needed to determine the difference in the K_2 parameter.
  - K_3 = 1.5606; this parameter was found to be the same as the global coefficient.
- Unbound layer calibration parameters:
  - Bs1 for coarse-grained soils = 0.40.
  - Bs1 for fine-grained soils = 0.40.

Figure 16 compares the predicted and measured rut depth using the Wyoming calibration coefficients for the LTPP and non-LTPP sections. As shown, the plots illustrate a reasonable fit and correspondence between the predicted and measured rut depths even when the sections with the irrational rut depth trends are included in the data. Figure 17 compares the predicted rut depth and residual rut depth errors and illustrates an unbiased transfer function or prediction model.

The irrational trends in rut depth for the new flexible pavement sections significantly increase the SEE or standard deviation between the measured and predicted total rut depth. Thus, the standard deviation relationship established from the global calibration study is recommended for use (see equations 23 to 25).

$$\sigma_{HMA} = 0.24\left(RD_{HMA}\right)^{0.8026} + 0.001 \quad (23)$$

$$\sigma_{Coarse-Grained} = 0.1477\left(RD_{Coarse-Grained}\right)^{0.6711} + 0.001 \quad (24)$$

$$\sigma_{Fine-Grained} = 0.1235\left(RD_{Fine-Grained}\right)^{0.5012} + 0.001 \quad (25)$$

Where:

σ_{HMA} = Standard deviation of the rut depth in all HMA layers.

$\sigma_{Coarse\text{-}Grained}$ = Standard deviation of the rut depth in the coarse-grained soils and aggregate base layers.
$\sigma_{Fine\text{-}Grained}$ = Standard deviation of the rut depth in the fine-grained soil layers.
RD_{HMA} = Average total predicted rut depth in the HMA layers.
$RD_{Coarse\text{-}Grained}$ = Average predicted rut depth in the coarse-grained soils layers.
$RDF_{ine\text{-}Grained}$ = Average predicted rut depth in the fine-grained soils.

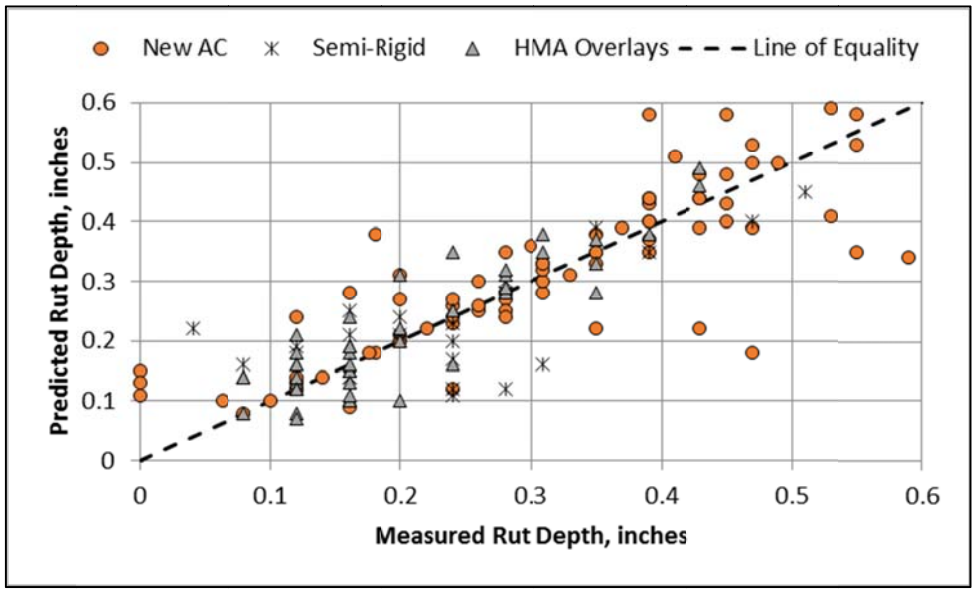

Figure 16—Predicted versus Measured Rut Depth using Wyoming's Calibration Coefficients

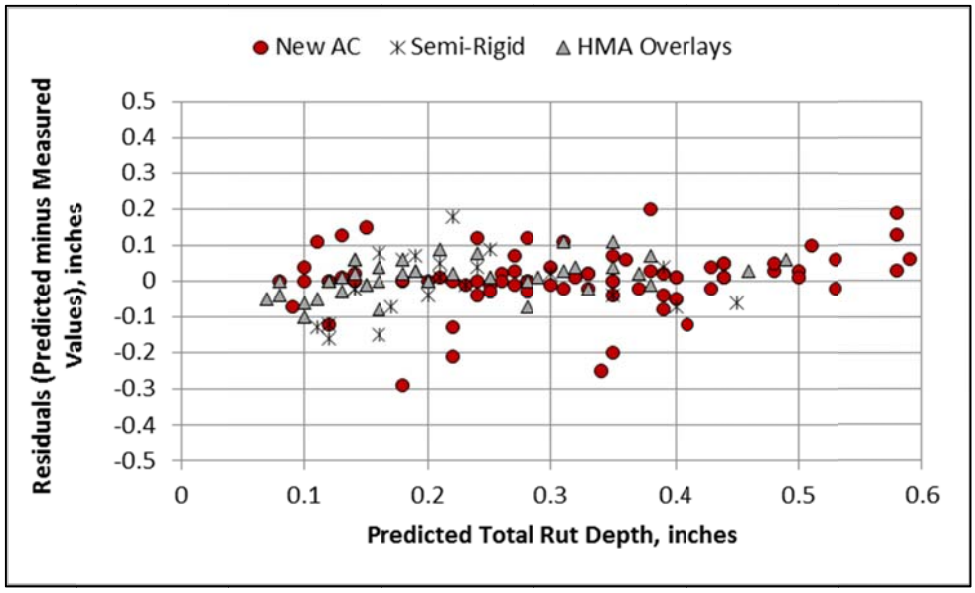

Figure 17—Residuals (Predicted minus Measured Values) versus Predicted Rut Depths for the WYDOT Calibration Coefficients

Figure 18 shows a comparison between the measured and predicted rut depths over time for three of the calibration sections. As shown, there are some anomalies or errors in the measured data (see sections 56-6029 and 56-6031 in figure 18). On the average, the WYDOT calibration coefficients provide a reasonable prediction of the total rut depth on the flexible and semi-rigid pavements.

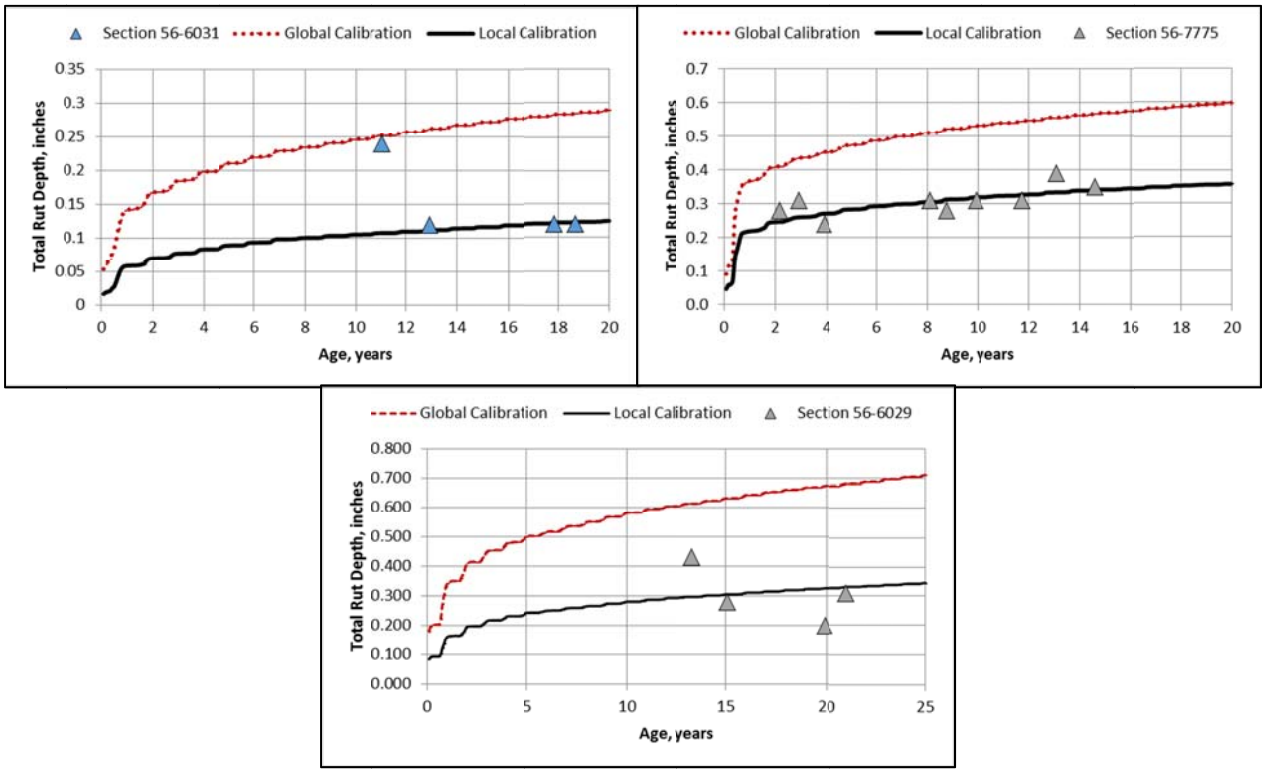

Figure 18—Predicted versus Measured Rut Depth over Time for Two Calibration Sections using Wyoming's Calibration Coefficients

4.2 Bottom-Up Area Fatigue Cracking

4.2.1 Transfer Function

Two types of load-related cracks are predicted by the MEPDG, alligator cracking and longitudinal cracking. The MEPDG assumes alligator or area cracks initiate at the bottom of the HMA layers and propagate to the surface with continued truck traffic, while longitudinal cracks are assumed to initiate at the surface.

The MEPDG Manual of Practice recommends that top-down or longitudinal cracking transfer function not be used to make design revisions, because of the debate and controversy on the appropriateness of the mechanism for surface initiated cracks and field investigations were not used to confirm longitudinal cracks initiated at the surface. Thus, only the bottom-up area fatigue relationship was used in the verification-calibration process.

The allowable number of axle load applications needed for the incremental damage index approach to predict both types of load related cracks (alligator and longitudinal) is shown below.

$$N_{f-HMA} = k_{f1}(C)(C_H)\beta_{f1}(\varepsilon_t)^{k_{f2}\beta_{f2}}(E_{HMA})^{k_{f3}\beta_{f3}} \quad (26)$$

Where:

$N_{f\text{-}HMA}$ = Allowable number of axle load applications for a flexible pavement and HMA overlays.

ε_t = Tensile strain at critical locations and calculated by the structural response model, in./in.

E_{HMA} = Dynamic modulus of the HMA measured in compression, psi.

k_{f1}, k_{f2}, k_{f3} = Global field calibration parameters (from the NCHRP 1-40D re-calibration; k_{f1} = 0.007566, k_{f2} = -3.9492, and k_{f3} = -1.281).

β_{f1}, β_{f2}, β_{f3} = Local or mixture specific field calibration constants; for the global calibration effort, these constants were set to 1.0.

$$C = 10^M \quad (27)$$

$$M = 4.84\left(\frac{V_{be}}{V_a + V_{be}} - 0.69\right) \quad (28)$$

V_{be} = Effective asphalt content by volume, percent.

V_a = Percent air voids in the HMA mixture.

C_H = Thickness correction term, dependent on type of cracking.

$$C_H = \frac{1}{0.000398 + \frac{0.003602}{1 + e^{(11.02 - 3.49 H_{HMA})}}} \quad (29)$$

H_{HMA} = Total HMA thickness, in.

The cumulative damage index (*DI*) is determined by summing the incremental damage indices over time, as shown below.

$$DI = \sum(\Delta DI)_{j,m,l,p,T} = \sum\left(\frac{n}{N_{f-HMA}}\right)_{j,m,l,p,T} \quad (30)$$

Where:

n = Actual number of axle load applications within a specific time period.

j = Axle load interval.

m = Axle load type (single, tandem, tridem, quad, or special axle configuration.

l = Truck type using the truck classification groups included in the MEPDG.

p = Month.

T = Median temperature for the five temperature intervals or quintiles used to subdivide each month, °F.

The area of alligator cracking and length of longitudinal cracking are calculated from the total damage over time using different transfer functions. The relationship used to predict the amount of alligator cracking on an area basis, FC_{Bottom}, is shown below.

$$FC_{Bottom} = \left(\frac{1}{60}\right)\left(\frac{C_4}{1+e^{\left(C_1C_1^*+C_2C_2^*Log\left(DI_{Bottom}*100\right)\right)}}\right) \quad (31)$$

Where:

FC_{Bottom} = Area of alligator cracking that initiates at the bottom of the HMA layers, percent of total lane area.

DI_{Bottom} = Cumulative damage index at the bottom of the HMA layers.

$C_{1,2,4}$ = Transfer function regression constants; C_4= 6,000; C_1=1.00; and C_2=1.00

$$C_1^* = -2C_2^* \quad (32)$$

$$C_2^* = -2.40874 - 39.748\left(1+H_{HMA}\right)^{-2.856} \quad (33)$$

H_{HMA} = Total HMA thickness, in.

4.2.2 Verification of the Global Calibration Coefficients

Area fatigue cracks (bottom-up cracks) for all HMA surfaced pavements were calculated with *Pavement ME Design*®. Figure 19 shows the predicted versus measured fatigue cracking using the global calibration coefficients for the sections in Wyoming and adjacent states. As shown, the MEPDG over predicts the area of fatigue cracking for most of the LTPP test sections located in adjacent states. Figure 20 shows the measured and predicted rut depths for just the Wyoming sections. Use of the global calibration coefficients results in a different observation; on the average, the MEPDG under predicts the amount of area fatigue cracks.

Figure 21 shows the fatigue cracking measured over time for the Wyoming new flexible sections, semi-rigid sections, and HMA overlaid sections. None of the LTPP semi-rigid pavement sections were located in the adjacent states (see table 3). Three important observations from this evaluation are listed below:

- The HMA overlaid sections exhibit the higher amounts of fatigue cracking earlier in the life of the overlay than the conventional flexible pavement sections, which is probably related to the occurrence of reflection cracks from the underlying surface.
- The semi-rigid sections exhibit the higher amounts of fatigue cracking over time in comparison to the conventional flexible pavement and HMA overlaid sections. The reason for the greater amounts of cracking is probably related to the occurrence of shrinkage cracks reflecting to the surface from the underlying cement treated base layer and/or the occurrence of debonding between the cement treated base and HMA layers.
- Most of the LTPP and non-LTPP sections exhibit low amounts of fatigue cracking. There was only one semi-rigid pavement section (56-2017) and one HMA overlaid section (56-2015) that exhibited more than 5 percent fatigue cracking over the life of the sections.

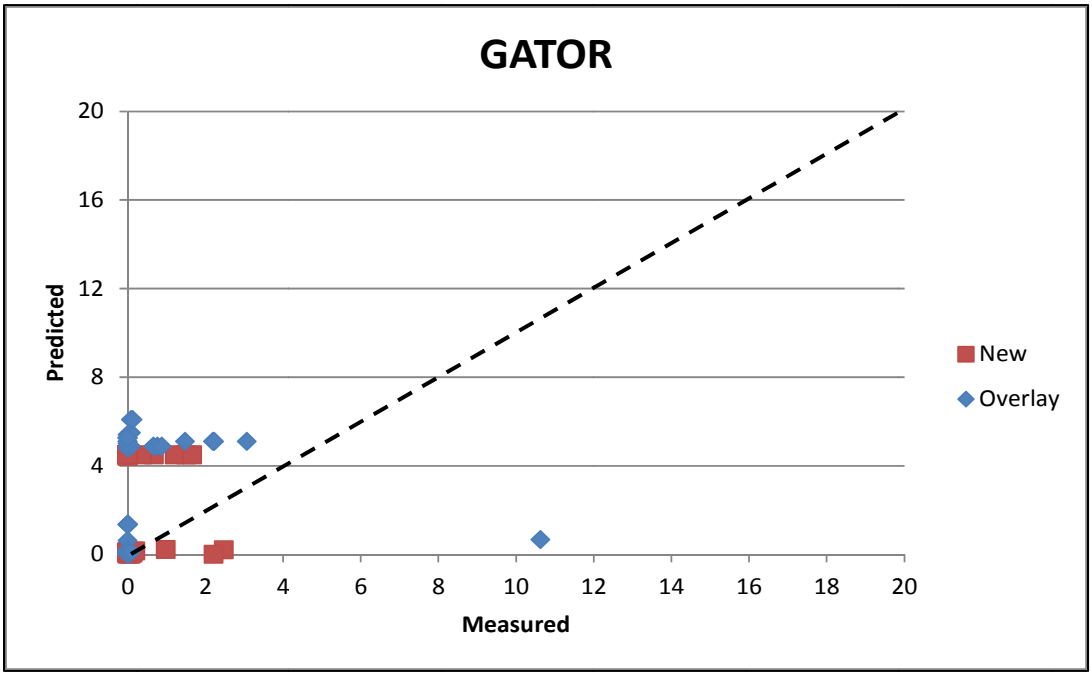

Figure 19—Predicted versus Measured Fatigue Cracking using the Global Calibration Coefficients

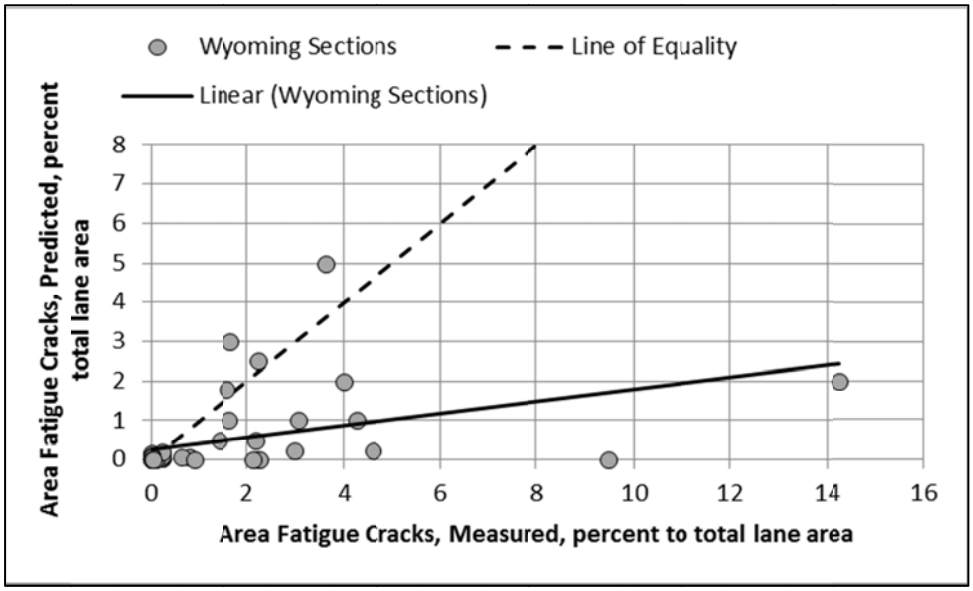

Figure 20—Predicted versus Measured Fatigue Cracking using the Global Calibration Coefficients for the Wyoming LTPP and Non-LTPP Sections

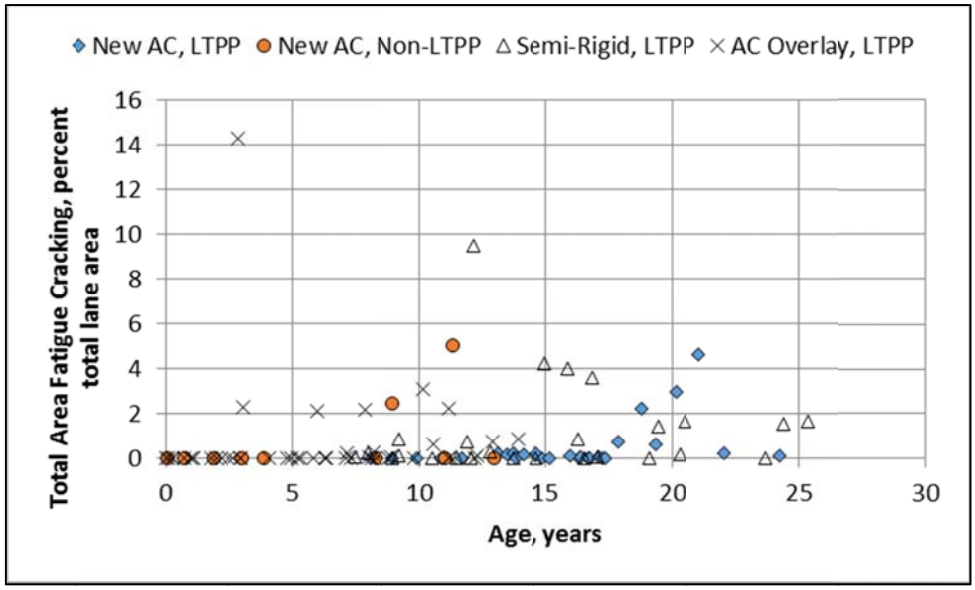

Figure 21—Area Fatigue Cracks Measured with Time for the Wyoming LTPP and Non-LTPP Sections

Figures 19 and 20 illustrate there is a bias in the predicted fatigue cracking and the goodness-of-fit is poor for the conventional flexible and semi-rigid pavements. The following lists some of the findings from the comparison of the predicted and measured amounts of fatigue cracking (see figures 19 and 20).

- The slope between the measured and predicted amounts or areas of fatigue cracking is significantly different than 1.0.
- The intercept is slightly higher than the origin.

4.2.3 Wyoming Calibration Coefficients

Measured fatigue cracking trends for each calibration section were carefully reviewed. The analysis utilized the full Wyoming flexible pavement database to establish the goodness of fit and bias in the MEPDG fatigue cracking transfer functions for the flexible and semi-rigid pavement sections.

The new flexible pavement sections were used to determine the adjustments to the HMA global calibration coefficients for fatigue cracking or the local calibration coefficients. The HMA local calibration coefficients from the new flexible pavement sections were then used for the semi-rigid sections to determine the calibration coefficients of the cement treated base layer, which will be discussed in the next section, and the reflection cracking calibration coefficients that will be discussed in a latter section of this chapter.

As noted above, the area of fatigue cracking exhibited on the flexible pavement sections were low so the WYDOT coefficients were assumed to be the same as the global fatigue cracking coefficients (see equation 26). The coefficients of the fatigue cracking transfer function between damage index and the area of cracking (see equation 31) were adjusted accordingly

to remove the bias shown in figure 20. The following summarizes the Wyoming calibration coefficients from this analysis, which were found to be independent on mixture type.

- Calibration coefficients for HMA mixture fatigue strength:
  - $K_1 = 0.00757$; this parameters has been found to be dependent on the amount of RAP included in the mixture. However, too few of the sections contained significantly different amounts of RAP to identify any difference within this parameter.
  - $K_2 = 3.9491$; this parameter is probably related to mixture type, but laboratory repeated load flexural fatigue tests are needed to determine the difference in the K_2 parameter.
  - $K_3 = 1.281$; this parameter was found to be the same as the global coefficient and independent of mixture type.
- Calibration coefficients for the bottom-up area fatigue cracking transfer function:
  - $C_1 = 0.4951$
  - $C_2 = 1.469$; this has been found to be greater than 2.0 for some western states. The reason for the lower C_2 parameter in Wyoming is unknown.
  - $C_3 = 6{,}000$

Figure 22 compares the predicted and measured fatigue cracking using the Wyoming calibration coefficients for the LTPP and non-LTPP sections. As shown, a reasonable fit (minimal bias but high standard deviation) and correspondence was obtained between the predicted and measured fatigue cracking of new flexible pavements. Figure 23 compares the predicted area of fatigue cracks and residual fatigue cracking errors and illustrates an unbiased transfer function and model.

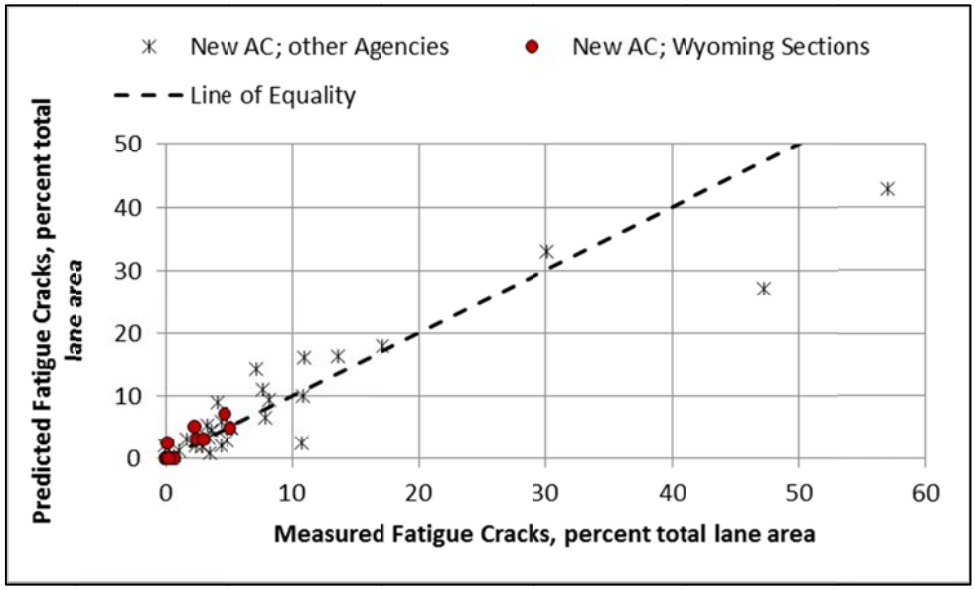

Figure 22—Predicted versus Measured Fatigue Cracking for the LTPP and Non-LTPP Sections using Wyoming's Calibration Coefficients

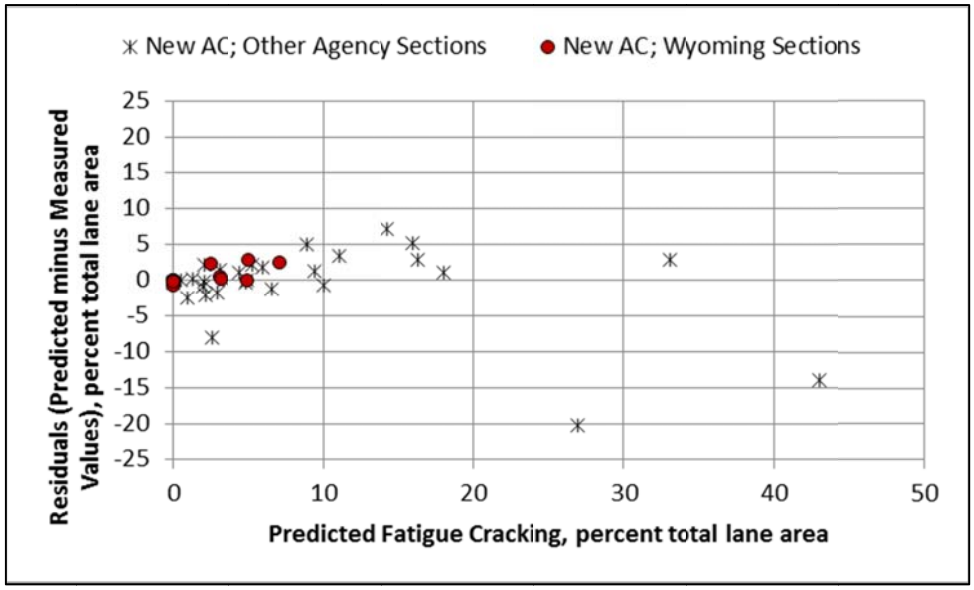

Figure 23—Residuals (Predicted minus Measured Values) versus Predicted Bottom-Up Fatigue Cracking for the WYDOT Calibration Coefficients

Area fatigue cracking for the WYDOT new flexible pavement sections are low compared to the area fatigue cracking measured for the LTPP sections in adjacent states. The difference or residual error between the predicted and measured values for the sections with the larger areas of fatigue cracking in the adjacent states could distort the standard deviation equation (see figure 23). Thus, the standard deviation relationship derived from the global calibration study is recommended for use (see equation 34).

$$\sigma_{Bottom-Up} = 1.13 + \frac{13}{1 + e^{(7.57 - 15.5 Log(FC_{Bottom-Up} + 0.0001))}} \quad (34)$$

Where:

$\sigma_{Bottom-Up}$ = Standard deviation of the area bottom-up fatigue cracking.
$FC_{Bottom-Up}$ = Bottom-up fatigue cracking damage index.

Figure 24 shows a comparison between the measured and predicted fatigue cracking over time for three of the WYDOT calibration sections. As shown, the WYDOT calibration coefficients provide a reasonable prediction of area fatigue cracking.

4.3 Fatigue Cracking of Semi-Rigid Pavements

4.3.1 Transfer Function

For fatigue cracks in CTB layers, the allowable number of load applications, $N_{f\text{-}CTB}$, is determined in accordance with equation 35 and the amount or area of fatigue cracking is calculated in accordance with equation 36. These damage and distress transfer functions were never calibrated under any of the NCHRP projects. Thus, the transfer function is provided below, but the coefficients are not recommended for use until the transfer function has been calibrated to the CTB materials and a specific climate.

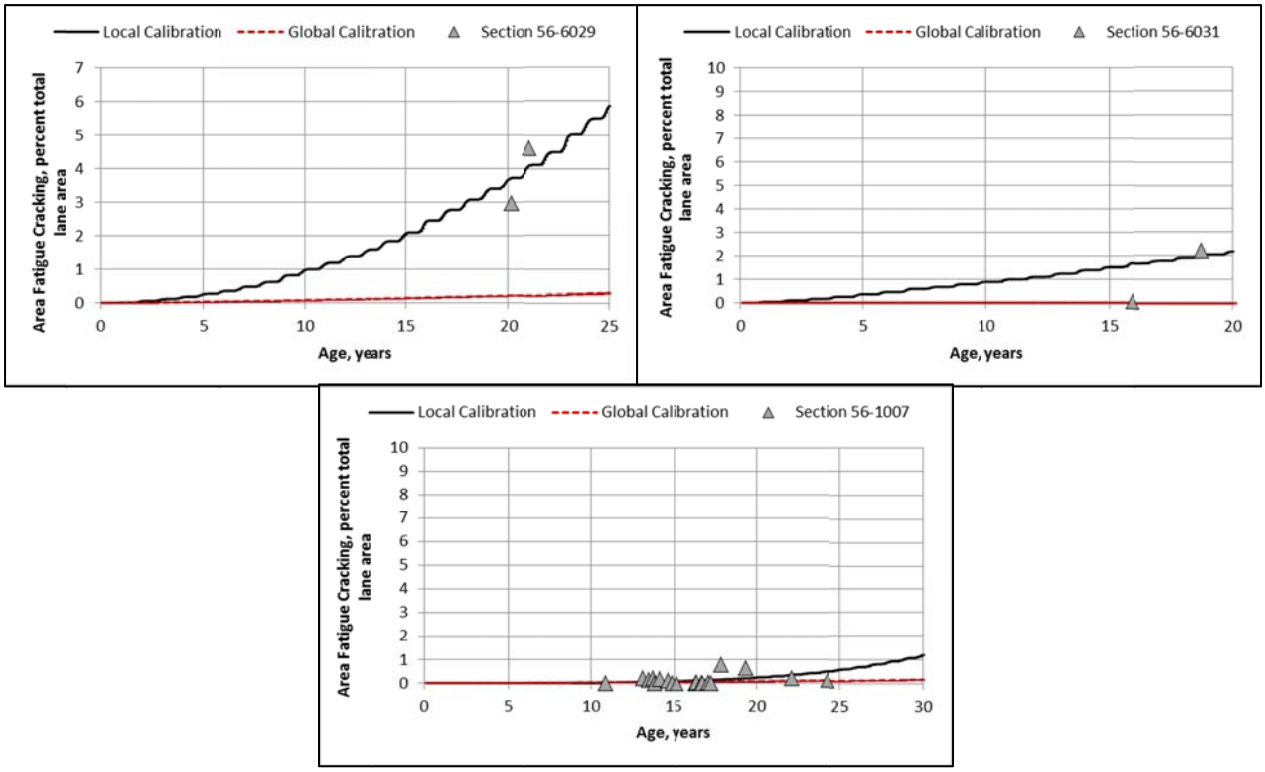

Figure 24—Predicted versus Measured Fatigue Cracking over Time for Selected Calibration Section using WYDOT's Calibration Coefficients

$$N_{f-CTB} = 10^{\left[\frac{k_{c1}\beta_{c1}\left(\frac{\sigma_t}{M_R}\right)}{k_{c2}\beta_{c2}}\right]} \quad (35)$$

$$FC_{CTB} = C_1 + \frac{C_2}{1+e^{(C_3 - C_4 Log(DI_{CTB}))}} \quad (36)$$

Where:

$N_{f\text{-}CTB}$ = Allowable number of axle load applications for a semi-rigid pavement.
σ_t = Tensile stress at the bottom of the CTB layer, psi.
M_R = 28-day Modulus of rupture for the CTB layer, psi.
DI_{CTB} = Cumulative damage index of the CTB or cementitious layer.
$k_{c1,c2}$ = Global calibration factors – Undefined because prediction equation was never calibrated; these values are set to 1.0 in the software. The Georgia and Montana DOTs have completed a local calibration study of fatigue cracking in semi-rigid pavements (Von Quintus, et al., 2007 and 2015). The calibration coefficients were found to be highly dependent on the condition or strength of the CTB layer. From other studies, k_{c1}=0.972 and k_{c2}=0.0825.
$\beta_{c1,c2}$ = Local calibration constants; these values are set to 1.0 in the software.
FC_{CTB} = Area of fatigue cracking, sq. ft.

$C_{1,2,3,4}$ = Transfer function regression constants; C_1=1.0, C_2=1.0, C_3=0, and C_4=1,000, however, this transfer function was never calibrated and these values will likely change once the transfer function has been calibrated.

The computational analysis of incremental fatigue cracking for a semi-rigid pavement uses the damaged modulus approach. In summary, the elastic modulus of the CTB layer decreases as the damage index, DI_{CTB}, increases. Equation 37 is used to calculate the damaged elastic modulus within each season or time period for calculating critical pavement responses in the CTB and other pavement layers.

$$E_{CTB}^{D(t)} = E_{CTB}^{Min} + \left(\frac{E_{CTB}^{Max} - E_{CTB}^{Min}}{1 + e^{(-4+14(DI_{CTB}))}} \right) \quad (37)$$

Where:

$E_{CTB}^{D(t)}$ = Equivalent damaged elastic modulus at time t for the CTB layer, psi.

E_{CTB}^{Min} = Equivalent elastic modulus for total destruction of the CTB layer, psi.

E_{CTB}^{Max} = 28-day elastic modulus of the intact CTB layer, no damage, psi.

4.3.2 Verification of the Global Calibration Coefficients

The semi-rigid fatigue strength and damage cracking relationships were never calibrated at the global level. Thus, the global coefficients for the semi-rigid transfer function were not used to predict the amount of fatigue cracking in semi-rigid pavements. The local calibration coefficients based on the results from Georgia, rather than Montana, were used as the starting point for the WYDOT values, because the Georgia calibration study used version 2.2 of the software (Von Quintus, et al., 2015).

4.3.3 Wyoming Calibration Coefficients

As noted above, only one of 14 semi-rigid pavement sections in Wyoming exhibited more than 5 percent fatigue cracks. Most of the new semi-rigid pavement sections exhibited less than 2 percent cracking. Figure 21 showed the amount of cracking exhibited over time for the new semi-rigid pavement sections, in comparison to the other LTPP and non-LTPP sections. Figure 25 shows the measured area fatigue cracking over time for the WYDOT LTPP and non-LTPP sections. As shown, many of the sections exhibit none or minimal area fatigue cracking over time.

The minimal amount of cracking reduces the confidence in the local calibration coefficients when the design criterion is more than 10 percent area fatigue cracking. The area of fatigue cracking for all of these sections is considered very small in comparison to typical design criterion, and thus, insufficient to complete a reliable calibration of the transfer function across a wider range of area fatigue cracking values.

The calibration coefficients of the semi-rigid fatigue cracking transfer function (see equation 35) are provided in table 9, while the transfer function calibration coefficients between cracking and damage (see equation 36) are listed below.

C_1 = 0.00
C_2 = 75 (theoretically this value should be close to 100)
C_3 = 5
C_4 = 3

These values, however, only confirm little to no fatigue cracking in the CTB exhibited through the evaluation period. The WYDOT calibration coefficients should be used with caution until more sections from Wyoming confirm the values.

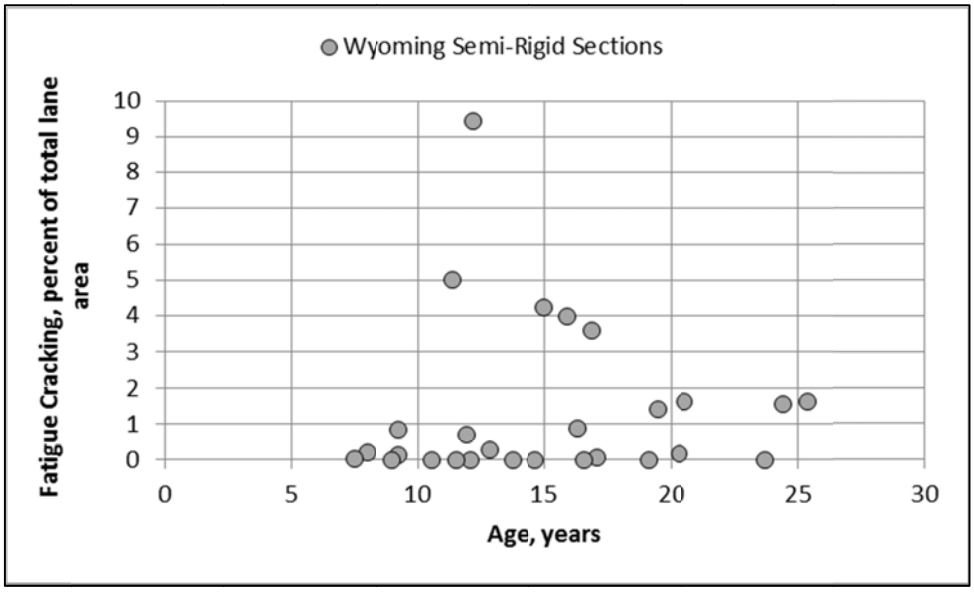

Figure 25—Measured Fatigue Cracking over Time for Wyoming's LTPP Sections

It is important to note that the occurrence of area fatigue cracks in the CTB was not measured for the LTPP and non-LTPP sections from any project (Georgia, Montana, etc.). The MEPDG predicts fatigue cracking in the HMA layer of a semi-rigid pavement using the reflection cracking transfer function and model. Thus, all of the semi-rigid pavement sections were used to determine the calibration coefficients of the reflection cracking transfer function, which is discussed in a latter section of this chapter.

In addition, no standard deviation equation was generated for the area fatigue cracking of the CTB layer for any of the local calibration studies previously referred to because the fatigue cracking of the CTB layer cannot be segregated from the area fatigue cracking of the HMA layer. Thus, the residual error or standard deviation equation for area fatigue cracking was determined from the reflection cracking predictions.

Table 9—Wyoming Semi-Rigid Pavement Fatigue Strength Calibration Coefficients

Condition or Type of CTB Layer	Coefficient in Semi-Rigid Fatigue Strength Equation (Equations 35)	
High Strength CTB (intact cores recovered with cement content greater than 6 percent; compressive strength generally greater than 1,000 psi)	B_{C1}	0.85
	B_{C2}	1.10
Moderate Strength CTB (intact cores recovered with cement contents greater than 4 percent but less than 6 percent; compressive strength generally greater than 300 psi but less than 1,000 psi)	B_{C1}	0.75
	B_{C2}	1.10
Low Strength CTB (intact cores cannot be recovered with cement content generally less than 4 percent; compressive strength generally less than 300 psi), similar to soil-cement	Semi-Rigid Pavement Simulation not applicable; assume conventional flexible pavement with high stiffness aggregate base layer.	

4.4 Thermal or Transverse Cracking

4.4.1 Transfer Function

The degree of cracking predicted by the MEPDG uses an assumed relationship between the probability distribution of the log of the crack depth to HMA layer thickness ratio and the percent of cracking. Equation 38 is used to determine the extent of thermal cracking.

$$TC = \beta_{t1} N\left[\frac{1}{\sigma_d} Log\left(\frac{C_d}{H_{HMA}}\right)\right] \quad (38)$$

Where:

TC = Observed amount of thermal cracking, ft/mi.
β_{t1} = Regression coefficient determined through global calibration (400).
$N[z]$ = Standard normal distribution evaluated at [z].
σ_d = Standard deviation of the log of the depth of cracks in the pavement (0.769), in.
C_d = Crack depth, in.
H_{HMA} = Thickness of HMA layers, in.

The crack depth or amount of crack propagation induced by a given thermal cooling cycle is predicted using the Paris law of crack propagation.

$$\Delta C = A(\Delta K)^n \quad (39)$$

Where:

ΔC = Change in the crack depth due to a cooling cycle.
ΔK = Change in the stress intensity factor due to a cooling cycle.
A, n = Fracture parameters for the HMA mixture, which are obtained from the indirect tensile creep-compliance and strength of the HMA in accordance with the following equations.

$$A = 10^{k_t \beta_t (4.389 - 2.52 Log(E_{HMA} \sigma_m n))} \quad (40)$$

Where:

$$\eta = 0.8\left[1 + \frac{1}{m}\right] \quad (41)$$

k_t = Coefficient determined through global calibration for each input level (Level 1 = 1.5; Level 2 = 0.5; and Level 3 = 1.5).
E_{HMA} = HMA indirect tensile modulus, psi.
σ_m = Mixture tensile strength, psi.
m = The m-value derived from the indirect tensile creep compliance curve measured in the laboratory.
β_t = Local or mixture calibration factor.

The stress intensity factor, K, is defined or estimated by the use of the following simplified equation.

$$K = \sigma_{tip}\left(0.45 + 1.99(C_o)^{0.56}\right) \quad (42)$$

Where:

σ_{tip} = Far-field stress from pavement response model at depth of crack tip, psi.
C_o = Current crack length, feet.

4.4.2 Verification of the Global Calibration Coefficients

The length of transverse cracks for all flexible and semi-rigid pavements was calculated with *Pavement ME Design*®. Figure 26 shows a comparison of the measured and predicted length of transverse cracks using the global calibration coefficients for all test sections in Wyoming and in adjacent states. As shown, there is a bias in the predicted length of transverse cracks and the goodness-of-fit is considered poor. Although the MEPDG has a limit on the predicted length of transverse cracks (2,112 ft./mi.), the MEPDG under predicts the length of transverse cracks. This observation has been reported by many other agencies (Mallela, et al., 2013; Darter, et al., 2009 and 2014; Von Quintus, et al., 2015).

Use of the global calibration coefficients resulted in very low lengths of transverse cracks. One reason for the biased predictions is low air voids and high effective asphalt contents by volume were reported for some of the WYDOT HMA mixtures. Lower air voids and higher asphalt contents result in smaller lengths of transverse cracks. However, the measured lengths of transverse cracks for the Wyoming sections are within the same range as the LTPP sections located in the adjacent states, which have much higher air voids and lower asphalt contents.

Figure 27 shows the length of transverse cracks measured over time for the new flexible sections located in Wyoming in comparison to those sections located in other agencies. No significant difference was identified between the length of transverse cracks measured on new flexible pavements in Wyoming and those located in other agencies. Figure 28 compares the length of transverse cracks measured over time for the new flexible sections, semi-rigid sections, and HMA overlaid sections. As shown, all family of pavement sections exhibited a similar range of measured values.

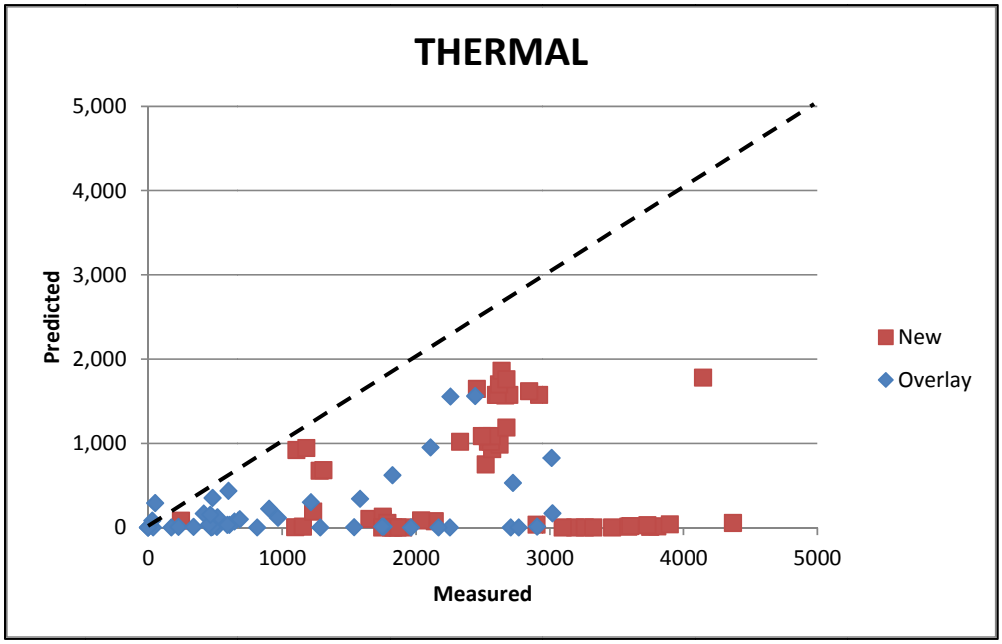

Figure 26—Predicted versus Measured Transverse Cracks using the Global Calibration Coefficients for Wyoming's LTPP and Non-LTPP Sections

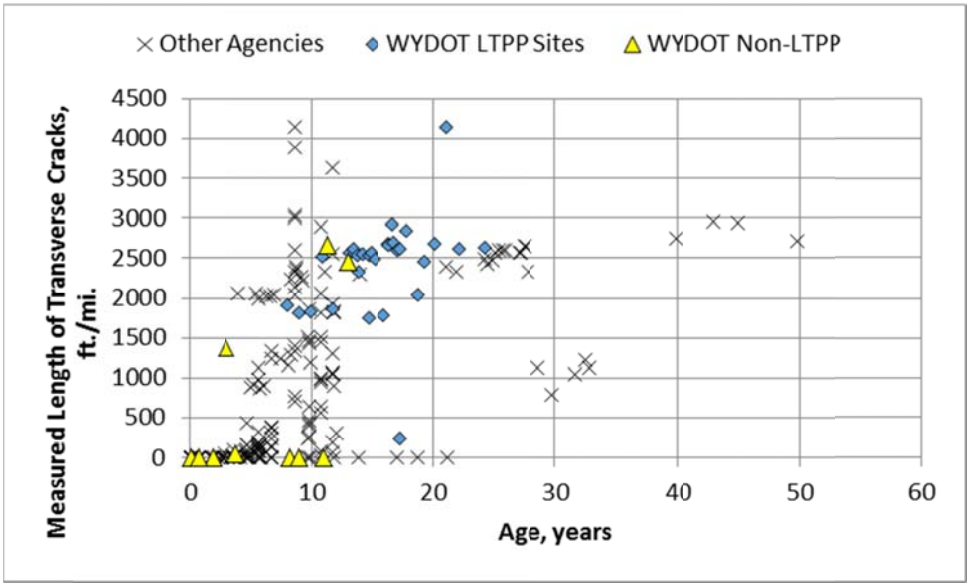

Figure 27—Length of Transverse Cracks Measured with Time for the Wyoming LTPP and Other Agency Sections

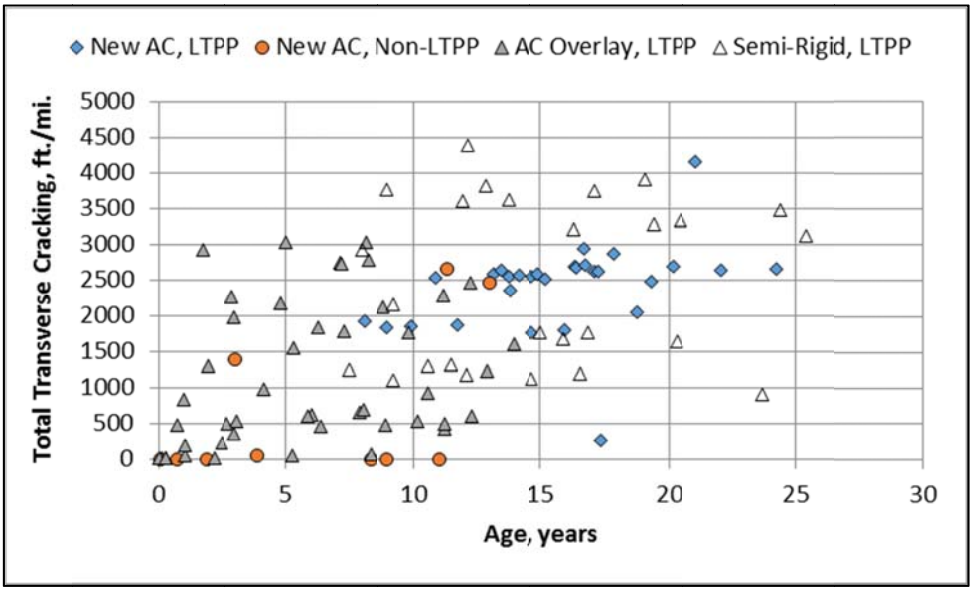

Figure 28—Length of Transverse Cracks Measured with Time for the Wyoming LTPP and Non-LTPP Sections

4.4.3 Wyoming Calibration Coefficients

The calibration process for the transverse cracking transfer function was restricted to new flexible pavements to exclude the possibility of transverse cracks reflecting through the HMA overlays of a flexible pavement and any transverse shrinkage cracks reflecting through the HMA surface of semi-rigid pavements. The LTPP flexible pavement sections with overlays and semi-rigid pavement sections were used to determine the input level 3 calibration coefficients for the reflection cracking transfer function. Indirect tensile creep compliance and strength properties were unavailable for all of the HMA mixtures placed on the WYDOT test sections and LTPP sections located in adjacent states.

Measured transverse cracking trends for each calibration section were reviewed. The analysis used all of the new flexible pavement sections in Wyoming and adjacent states to establish the goodness of fit and bias for the transverse cracking transfer function. Two calibration coefficients were derived to remove the bias using input level 3: a K_{t3} value of 7.5 for the Wyoming sites and a K_{t3} value of 5.5 for the sites located in adjacent states. Some of the LTPP sites located in adjacent states exhibited transverse cracking a little earlier than the WYDOT sites (see figure 27), but the effective asphalt content by volume is much higher and the air voids lower for the WYDOT sites.

Figure 29 compares the predicted and measured lengths of transverse cracks for the new flexible sections. The LTPP test sections in Wyoming exhibit the higher lengths of transverse cracks, while the non-LTPP section exhibit much lower lengths of cracking. One reason for this difference is that the LTPP sections are much older than the non-LTPP sections.

Figure 30 compares the predicted length of transverse cracks and residual errors of transverse cracks and illustrates an unbiased transfer function and model. However, there is a large dispersion (standard error) between the predicted and measured values for a couple of reasons.

- One reason for this high dispersion is the cause of the transverse cracks is probably not from a low temperature event but a combination of shrinkage and lower temperatures. The MEPDG only predicts the length of transverse cracks caused by low temperature events.
- Another reason is that the maximum length of transverse cracks predicted by the MEPDG is 2,112 ft./mi.

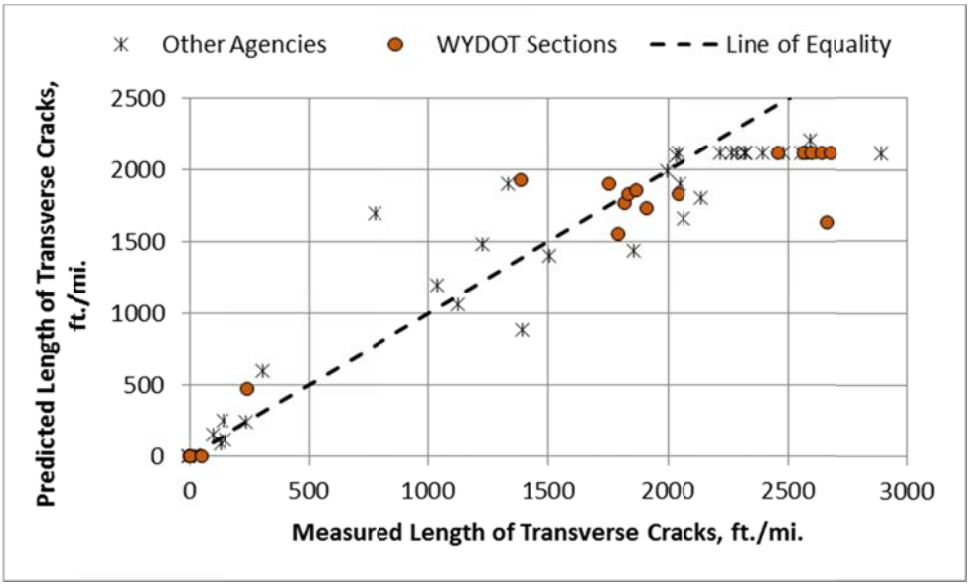

Figure 29—Predicted versus Measured Length of Transverse Cracks for the LTPP and Non-LTPP Sections using Wyoming's Calibration Coefficients

As such, the standard deviation relationship derived from the global calibration effort is recommended for use (see equation 43). In addition, it is suggested that a 50 percent reliability level be used in design because of the high standard deviation of the residuals.

$$\sigma_{TC3} = 0.3972(TC_L) + 20.422 \quad (43)$$

Where:

σ_{TC3} = Standard deviation of the length of predicted transverse cracks.
TC_L = Average length of the predicted transverse cracks.

Figure 31 shows a comparison between the measured and predicted lengths of transverse cracks over time for two of the LTPP calibration sections located in Wyoming. On the average, the WYDOT calibration coefficients provide a reasonable prediction of the length of transverse cracks for the flexible pavements.

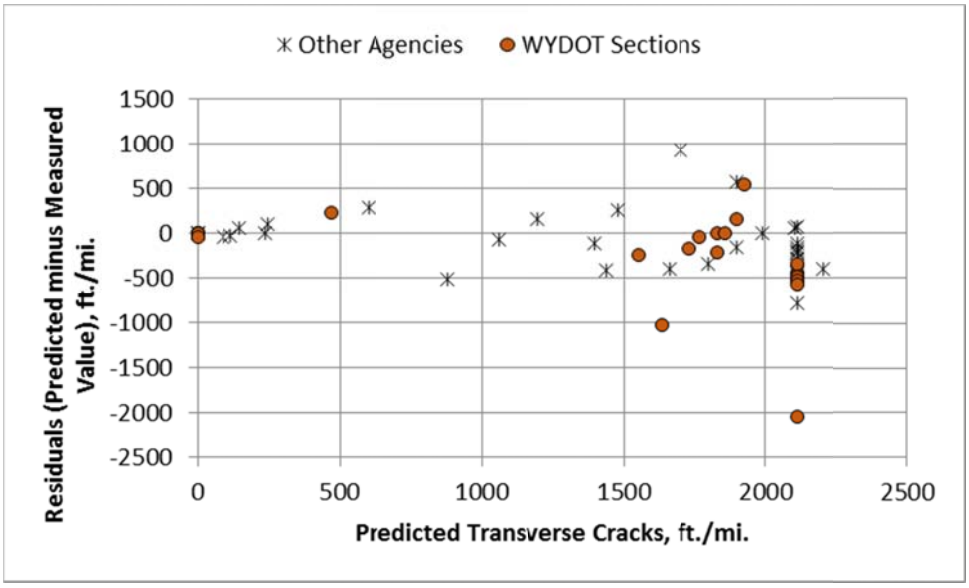

Figure 30—Residuals (Predicted minus Measured Values) versus Predicted Transverse Cracking for the WYDOT Calibration Coefficients

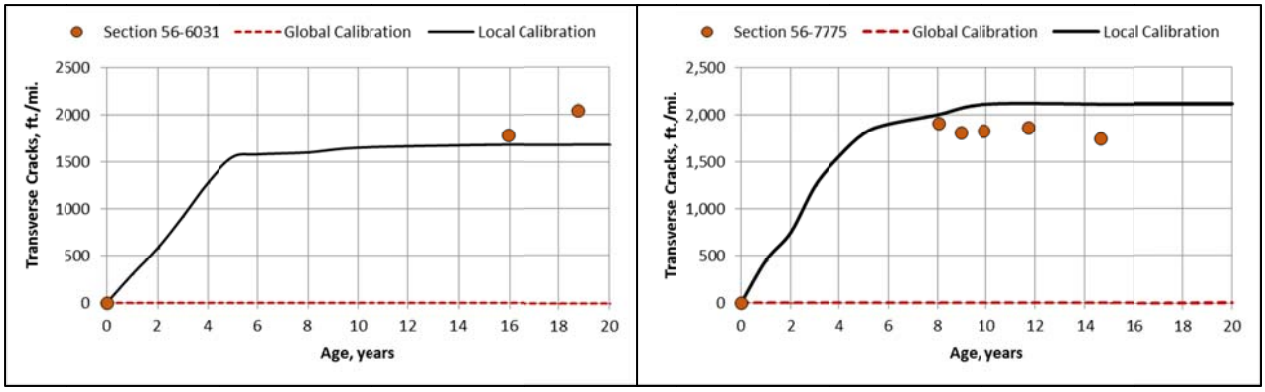

Figure 31—Predicted versus Measured Length of Transverse Cracks over Time for Selected Calibration Section using Wyoming's Calibration Coefficients

4.5 Reflection Cracking—HMA Overlays

4.5.1 Transfer Functions

Version 2.2 of the MEPDG software predicts reflection cracks in an HMA overlay and HMA surface of semi-rigid pavements using a fracture mechanics-based model. The Paris-Erdogan's law is used to model crack propagation, as expressed in equation 44, and is similar to the one used to predict transverse cracks. The model is used for estimating the amount of area fatigue and thermal cracks from a non-surface layer that reflects to the surface after a certain period of time.

$$\frac{dc}{dN} = A(\Delta K)^n \qquad (44)$$

Where:

c = Crack length and dc is the change or growth in crack length.
N = Number of loading cycles and dN is the increase in loading cycles during a time increment.
ΔK = Stress intensity amplitude that depends on the stress level, the geometry of the pavement structure, the fracture model, and crack length.
A,n = Fracture properties of the asphalt concrete mixture.

The fracture properties A and n are calculated from the indirect tensile creep-compliance and strength of the asphalt concrete mixture in accordance with equations 45 and 46.

$$A = g_2 = \frac{g_3}{m_{mix}}\left(LogD_1\right) + g_4 \log \sigma_t \tag{45}$$

$$n = g_0 + \frac{g_1}{m_{mix}} \tag{46}$$

Where:

g_0,g_1,g_2,g_3,g_4 = Regression or calibration coefficients.
m_{mix} = The log-log slope of the mixture modulus versus loading time relationship for the current temperature and loading time.
D_1 = Coefficient of the creep compliance expressed in the power law form.
σ_t = Tensile strength of the asphalt concrete mix at the specific temperature.

Three modes of loading are used to propagate the cracks on a daily and/or monthly basis. The following equations define the crack propagation for the three mechanisms or modes of loading.

$$dc_{bending} = \sum A\left(\Delta K_{bending}\right)^n \frac{w_{bending}}{SF_{bending}} \tag{47}$$

$$dc_{shearing} = \sum A\left(2\Delta K_{bending}\right)^n \frac{w_{shearing}}{SF_{shearing}} \tag{48}$$

$$dc_{thermal} = \sum A\left(\Delta K_{thermal}\right)^n \tag{49}$$

Where:

SF = Healing shift function to account for the rest period between load cycles.

$$SF_{healing} = 1 + g_5\left(\frac{\Delta t_{rest}}{a_t}\right)^{g_6} \tag{50}$$

Δt_{rest} = Rest period between load cycles or applications.
a_t = Shift factor.

After HMA overlay placement, the underlying bound layers (all HMA, asphalt bound layers, chemically stabilized layers, and PCC layers) undergo load-related damage with continued truck loadings. The continual fatigue damage accumulation of these layers is considered in the MEPDG HMA overlay analysis procedure. For any given month, *m*, the total fatigue damage is estimated by equation 51.

$$DI_m = \sum_{i=1}^{m} \Delta DI_i \quad (51)$$

Where:

DI_m = Damage index for month *m*.
ΔDI_i = Increment of damage index in month *i*.

The area of fatigue damage for the underlying layer at month m (CA_m) is given by equation 52.

$$CA_m = \frac{100}{1 + e^{6-(6DI_m)}} \quad (52)$$

For each month *i*, there will be an increment of damage ΔDI_i which will cause an increment of cracking area CA_i to the stabilized layer. To estimate the amount of cracking reflected from the stabilized layer to the surface of the pavement for month m, the reflective cracking prediction equation is applied incrementally, in accordance with equation 53.

$$TRA_m = \sum_{i=1}^{m} RC_t\left(\Delta CA_i\right) \quad (53)$$

Where:

TRA_m = Total reflected cracking area for month m.
RC_t = Percent cracking reflected for age *t* (in years).
ΔCA_i = Increment of fatigue cracking for month i.

$$RC = \frac{100}{1 + e^{a(c)+bt(d)}} \quad (54)$$

Where:

RC = Percent of cracks reflected. [NOTE: The percent area of reflection cracking is output with the width of cracks being 1 ft.]
t = Time, years.
a, b = Regression fitting parameters defined through calibration process.
c,d = User-defined cracking progression parameters.

4.5.2 Verification of the Global Calibration Coefficients

As noted above, the reflection cracking transfer function and model included in version 2.2 of the software replaced the regression equation in the earlier versions. Thus, the global calibration factors were determined using a different data set than for the other transfer functions.

The HMA overlays and semi-rigid pavements were used to determine the reflection cracking global calibration coefficients by AASHTO prior to the release of version 2.2. The values summarized in table 10 were used as part of predicted the measured values for fatigue cracking of HMA layers and cement treated layers, transverse cracks from HMA layers, and shrinkage cracks in cement treated layers.

Table 10—Global Calibration Coefficient for HMA Overlays and HMA Surfaces of Semi-Rigid Pavements

Calibration Coefficient	New Semi-Rigid Pavements		HMA Overlays of Flexible and Semi-Rigid Pavements	
	Fatigue Cracking	Transverse Cracking	Fatigue Cracking	Transverse Cracking
K1	0.45	0.45	0.012	0.012
K2	0.05	0.05	0.005	0.005
K3	1.0	1.0	1.0	1.0
C1	1.64	0.1	0.38	3.22
C2	1.1	0.9809	1.66	25.7
C3	0.19	0.19	2.72	0.1
C4	62.1	165.3	105.4	133.4
C5	-404.6	-5.1048	-7.02	-72.4
m-Value	---	120	---	---

Figure 32 provides a comparison between the measured and predicted area fatigue cracks for the LTPP sections with HMA overlays and for semi-rigid pavements in comparison to the new flexible pavement sections. Figure 33 provides a similar comparison exceed between the measured and predicted length of transverse cracks. In summary, the global calibration coefficients were found to be applicable to Wyoming conditions and rehabilitation strategies.

In addition, the standard deviation relationships established from the global calibration process is recommended for use because there are too few test sections to account for the anomalies and irrational trends in the measured values for some of the sections. Table 11 summarizes the standard deviation relationships for reflection cracking for each pavement type and design strategy.

Table 11—Standard Deviation Relationships for Reflection Cracking

Pavement Type	Standard Deviation Relationship for:	
	Fatigue Cracking	Transverse Cracking
New Semi-Rigid Pavements	$\sigma = 1.3897(FC_T)^{0.296} + 0.4212$ (Equation 55)	$\sigma = 0.000027(TC_L)^{2.1187} + 399.9$ (Equation 56)
AC Overlay of Semi-Rigid and Flexible Pavements	$\sigma = 1.1097(FC_T)^{0.6804} + 1.23$ (Equation 57)	$\sigma = 70.98(TC_L)^{0.2994} + 30.12$ (Equation 58)

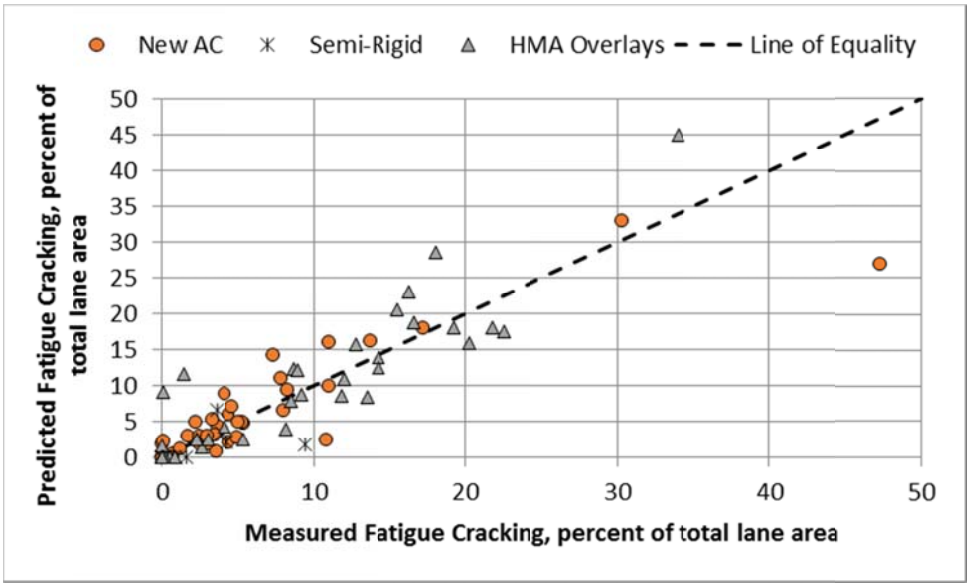

Figure 32—Predicted versus Measured Total Fatigue Cracking (Reflected Cracks plus New Fatigue Cracks) for the LTPP and Non-LTPP Sections using Wyoming's Calibration Coefficients

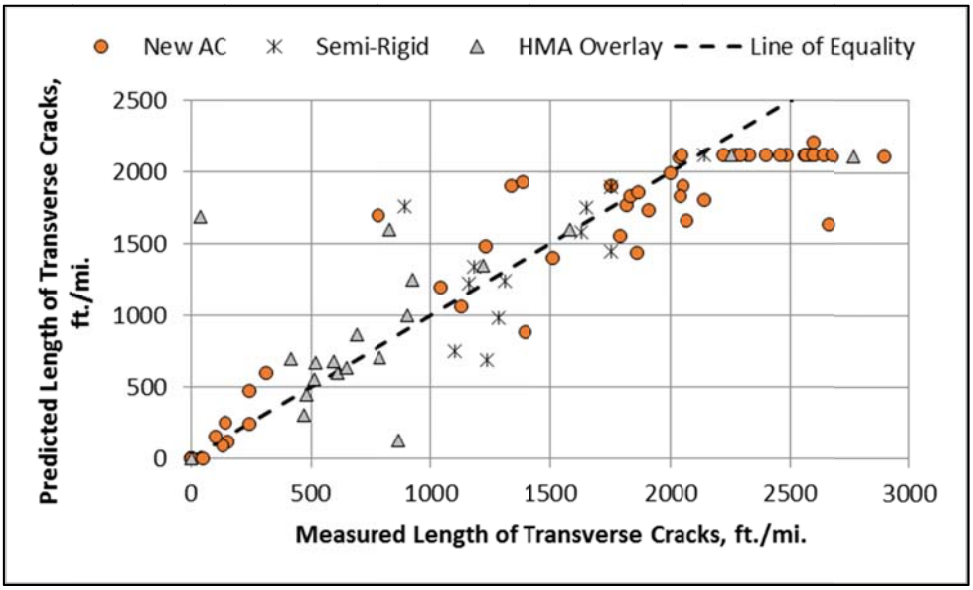

Figure 33—Predicted versus Measured Total Length of Transverse Cracking (Reflected Cracks plus New Transverse Cracks) for the LTPP and Non-LTPP Sections using Wyoming's Calibration Coefficients

4.6 IRI or Smoothness

4.6.1 Regression Equation

The following equations were developed from data collected within the LTPP program and are used to predict IRI over time for HMA-surfaced pavements.

Equation for New HMA Pavements and HMA Overlays of Flexible Pavements:

$$IRI = IRI_o + C_4(SF) + C_2(FC_{Total}) + C_3(TC) + C_1(RD) \quad (59)$$

Where:

IRI_o = Initial IRI after construction, in./mi.
SF = Site factor; as defined below.
FC_{Total} = Area of fatigue cracking (combined alligator, longitudinal, and reflection cracking in the wheel path), percent of total lane area. All load related cracks are combined on an area basis – length of cracks is multiplied by 1 foot to convert length into an area basis.
TC = Length of transverse cracking (including the reflection of transverse cracks in existing HMA pavements), ft/mi.
RD = Average rut depth, in.
$C_{1,2,3,4}$ = Coefficients from the regression analysis (see table 12).

The site factor (SF) is calculated in accordance with the following equation.

$$SF = Age(0.02003(PI + 1) + 0.007947(\mathrm{Pr}\,ecip + 1) + 0.000636(FI + 1)) \quad (60)$$

Where:

Age = Pavement age, years.
PI = Percent plasticity index of the soil.
FI = Average annual freezing index, degree F days.
$Precip$ = Average annual precipitation or rainfall, in.

Equation for HMA Overlays of Rigid Pavements:

$$IRI = IRI_o + C_4(SF) + C_2(FC_{Total}) + C_3(TC) + C_1(RD) \quad (61)$$

Table 12—Global Calibration Coefficients for New Flexible Pavements, HMA Overlays of Flexible and Semi-Rigid Pavements, and HMA Overlays of JPCP

Coefficient in Regression Equations (equations 59 and 61)		New Flexible Pavement and HMA Overlay of Flexible and Semi-Rigid Pavement	HMA Overlays of Rigid Pavements
C1	Rut Depth	40	40.8
C2	Fatigue Cracking	0.4	0.575
C3	Transverse Cracking	0.0008	0.014
C4	Site Factor	0.015	0.00825

4.6.2 Verification of the Global Calibration Coefficients

The IRI values measured on the LTPP test sections were evaluated and compared to determine if bias or significant differences exist between the different sets of data. Figure 34 includes a comparison of the IRI measured over time for the different sets of data. The new flexible pavements consistently exhibit smoother pavements or lower IRI values. Figure 35 compares the IRI measured over time between the LTPP sections location in Wyoming and those located in other states. As shown, no difference was identified between the sections located in Wyoming and in adjacent states.

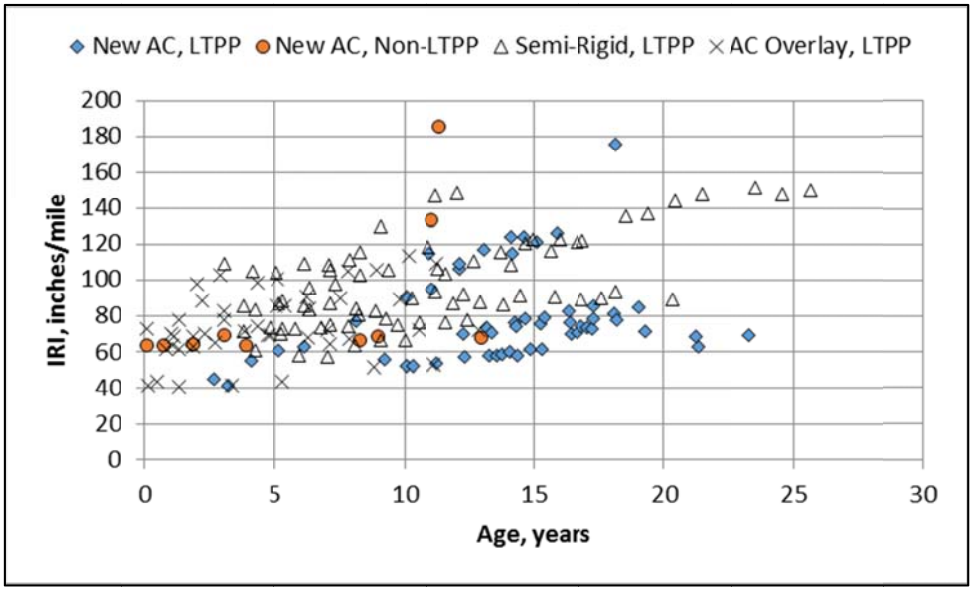

Figure 34—Measured IRI over Time for Flexible, Semi-Rigid, and HMA Overlay Pavements

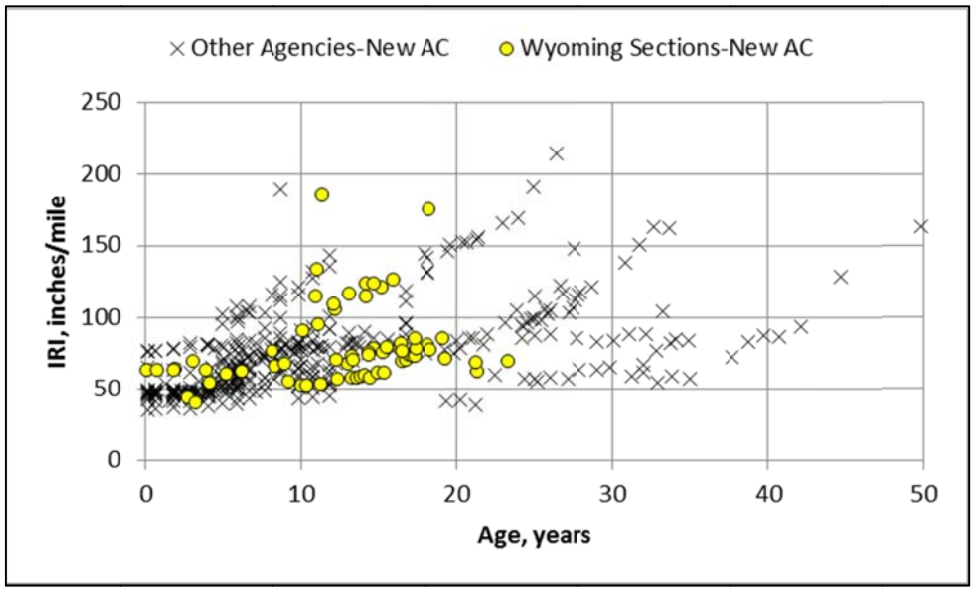

Figure 35—Measured IRI over Time for New Flexible Pavements in Wyoming and Adjacent States

Figure 36 includes a comparison of the predicted and measured IRI values for the Wyoming LTPP sites using the global calibration coefficients (see table 12) and the adjusted distress predictions using the local calibration coefficients for the other distresses. As shown, there is an insignificant bias in the predicted IRI values. In summary, the global calibration coefficients for the IRI regression equations were found to be applicable to the pavement structures used in the Wyoming calibration study after the other pavement distress predictions were adjusted to remove any bias. Thus, the global calibration coefficients are recommended for use.

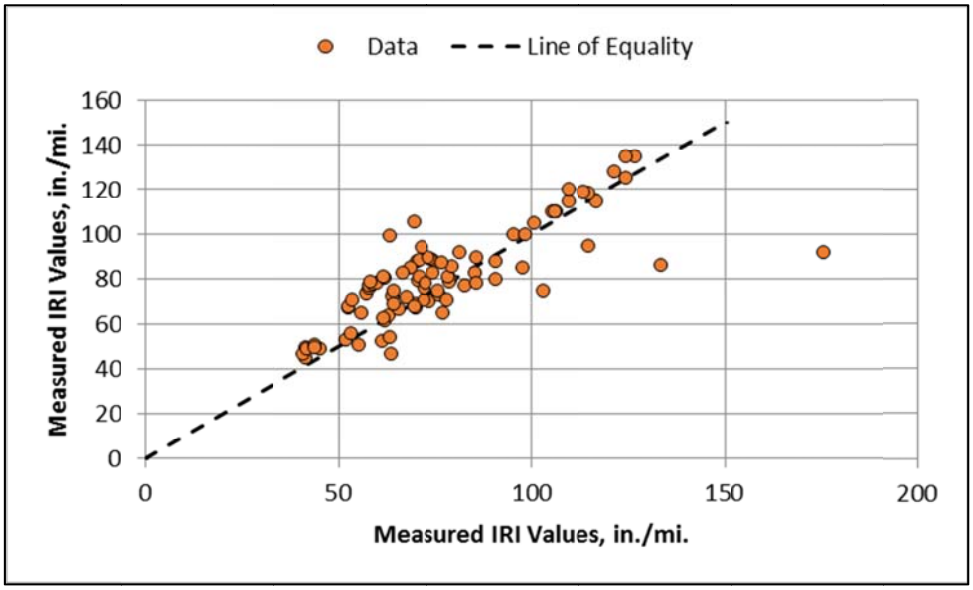

Figure 36—Measured IRI over Time for New Flexible Pavements in Wyoming and Adjacent States

CHAPTER 5 — SUMMARY AND CONCLUSIONS

5.1 Major and Appropriate Findings

The following summarize the major and important findings relative to the calibration of the MEPDG transfer functions to the design features and site conditions found in Wyoming.

- The number of LTPP sites located in Wyoming for rigid, flexile, and semi-rigid pavements were insufficient to determine the calibration coefficients of the transfer functions. LTPP sites in adjacent states and non-LTPP sites located in Wyoming were needed for the study. In summary, 26 JPCP sections were used, 14 semi-rigid sections, and 86 flexible pavement sections were used to adjust the calibration coefficients of the transfer functions to reasonably predict pavement distress and performance.

- The 2010 AASHTO MEPDG Local Calibration Guide was followed in verifying the global calibration coefficients and in calibrating the new calibration coefficients.

- The magnitude of the JPCP percent cracked slabs was too low to accurately define the calibration coefficients for mid-slab cracking.

- The calibration coefficients for the IRI regression equations for both flexible and rigid pavements were found to result in unbiased predictions of smoothness.

- Over 50 percent of the LTPP new flexible pavement sections exhibited irrational trends in the measured rut depths over time.

- The flexible and semi-rigid pavement sections exhibited low magnitudes of fatigue cracking.

5.2 Wyoming Calibration Coefficients

Both LTPP and non-LTPP test sections were used to estimate the precision and bias of the MEPDG transfer functions for predicting the performance indicators (distress and roughness) of WYDOT's pavements. The resulting distress prediction models, or transfer functions, can be used to optimize new pavement and rehabilitation design strategies, and used in forecasting of maintenance, repair, rehabilitation, and reconstruction costs.

The remainder of this section lists the WYDOT calibration factors for each transfer function for both flexible and rigid pavements. Tables 13 to 19 list the appropriate flexible and semi-rigid pavement WYDOT calibration factors from the local calibration study, while tables 20 to 22 list the appropriate rigid pavement (JPCP) calibration factors.

Table 13—WYDOT Calibration Coefficients for Asphalt Concrete Rut Depth Transfer Function

Transfer Function Coefficient	Global Value	WYDOT Value
K1	-3.35412	-2.45
K2	1.5606	No change
K3	0.4791	0.30
Standard Deviation	$0.24 * Pow(RD, 0.80519) + 0.001$	No change
RD = Average rut depth predicted by the Pavement ME Design software.		

Table 14—WYDOT Calibration Coefficients for Unbound Layers Rut Depth Transfer Function

Transfer Function Coefficient	Global Value	WYDOT Value
Coarse-Grained, Bs1	1.0	0.40
Fine-Grained, Bs1	1.0	0.40
Standard Deviation; Coarse-Grained Soil	$\sigma_{Coarse-Grained} = 0.1477\left(RD_{Coarse-Grained}\right)^{0.6711} + 0.001$	No change
Standard Deviation; Fine-Grained Soil	$\sigma_{Fine-Grained} = 0.1235\left(RD_{Fine-Grained}\right)^{0.5012} + 0.001$	No change
NOTE: The standard deviation equation is unchanged. All of the variance or variability was included in the HMA rut depth prediction equation.		

Table 15—WYDOT Calibration Coefficients for Flexible Pavement Bottom-Up Fatigue Cracking Transfer Function

Transfer Function Coefficient	Global Value	WYDOT Value
K1	0.007566	No change
K2	3.9492	No change
K3	1.281	No change
C1	1.0	0.4951
C2	1.0	1.469
C3	6,000	No change
Standard Deviation	$\sigma_{Bottom-Up} = 1.13 + \frac{13}{1 + e^{\left(7.57 - 15.5 Log\left(FC_{Bottom-Up} + 0.0001\right)\right)}}$	No change
DI_{Bottom} – Damage index for bottom up fatigue or alligator cracking.		

Table 16—WYDOT Calibration Coefficients for Asphalt Concrete Thermal Transverse Cracking Transfer Function

Transfer Function Coefficient	Global Value	WYDOT Value
Bt1	1.5	Not defined; because no laboratory tests.
Bt3	1.5	7.5
Standard Deviation (input level 3)	$\sigma_{TC3} = 0.3972(TC_L) + 20.422$	No change.
NOTE: The standard deviation equation remains unchanged because of the high variability and it is recommended that 50 percent reliability be used. If 50 percent reliability is used, the standard deviation has no effect on the final results.		

Table 17—WYDOT Calibration Coefficients for Semi-Rigid Pavement Fatigue Cracking Transfer Function

Transfer Function Coefficient	Condition or Type of CTB Layer	Global Value	WYDOT Value
B_{C1}	High Strength CTB (intact cores recovered with cement content greater than 6 percent; compressive strength generally greater than 1,000 psi)	Not Calibrated	0.85
B_{C2}		Not Calibrated	1.10
B_{C1}	Moderate Strength CTB (intact cores recovered with cement contents greater than 4 percent but less than 6 percent; compressive strength generally greater than 300 psi but less than 1,000 psi)	Not Calibrated	0.75
B_{C2}		Not Calibrated	1.10
	Low Strength CTB (intact cores cannot be recovered with cement content generally less than 4 percent; compressive strength generally less than 300 psi), similar to soil-cement	Semi-Rigid Pavement Simulation not applicable; assume conventional flexible pavement with high stiffness aggregate base layer.	
C1	Not defined by type or condition of CTB layer.	Not Calibrated	0.00
C2	Not defined by type or condition of CTB layer.	Not Calibrated	75
C3	Not defined by type or condition of CTB layer.	Not Calibrated	5
C4	Not defined by type or condition of CTB layer.	Not Calibrated	3
Standard Deviation		Not Calibrated	NA
NOTE: The standard deviation equation was not defined because the global calibration process was not completed under the NCHRP project. However, the CTB fatigue cracks were not segregated from the new fatigue cracking in the HMA surface, so a 50 percent reliability level is recommended for use. If 50 percent reliability is used, the standard deviation has no effect on the final results.			

Table 18—WYDOT Calibration Coefficient for Fatigue and Transverse Reflection Cracking in HMA Overlays and HMA Surfaces of Semi-Rigid Pavements

Calibration Coefficient	Global Calibration	Local Calibration			
		New Semi-Rigid Pavements		HMA Overlays of Flexible and Semi-Rigid Pavements	
		Fatigue Cracking	Transverse Cracking	Fatigue Cracking	Transverse Cracking
K1	Transfer functions were changed, so global calibration not applicable.	0.45	0.45	0.012	0.012
K2		0.05	0.05	0.005	0.005
K3		1.0	1.0	1.0	1.0
C1		1.64	0.1	0.38	3.22
C2		1.1	0.9809	1.66	25.7
C3		0.19	0.19	2.72	0.1
C4		62.1	165.3	105.4	133.4
C5		-404.6	-5.1048	-7.02	-72.4
m-Value		---	120	---	---

Table 19—WYDOT Calibration Coefficients for IRI Regression Equation for New Flexible Pavements, HMA Overlays of Flexible and Semi-Rigid Pavements, and HMA Overlays of JPCP

Coefficient in Regression Equations		New Flexible Pavement and HMA Overlay of Flexible and Semi-Rigid Pavement		HMA Overlays of Rigid Pavements	
		Global Value	WYDOT Value	Global Value	WYDOT Value
C1	Rut Depth	40	No change	40.8	No change
C2	Fatigue Cracking	0.4	No change	0.575	No change
C3	Transverse Cracking	0.0008	No change	0.014	No change
C4	Site Factor	0.015	No change	0.00825	No change

Table 20—WYDOT Calibration Coefficients for JPCP Mid-Slab Cracking Transfer Function

Transfer Function Coefficient	Global Value	WYDOT Value
C1	2.0	No change
C2	1.22	No change
C4	0.52	No change
C5	-2.17	No change
Standard Deviation	3.5522*Pow(CRACK,0.3415)+0.75	No change.

Table 21—WYDOT Calibration Coefficients for JPCP Faulting Transfer Function

Transfer Function Coefficient	Global Value	WYDOT Value
C1	0.595	0.5104
C2	1.636	0.00838
C3	0.00217	0.00147
C4	0.00444	0.08345
C5	250	5999
C6	0.47	0.504
C7	7.30	5.9293
C8	400	400
Standard Deviation	0.07162*Pow(FAULT,0.368)+0.00806	0.0831*Pow(FAULT,0.3426)+0.00521

Table 22—WYDOT Calibration Coefficients for JPCP IRI Transfer Function

Transfer Function Coefficient	Global Value	WYDOT Value
J1	0.8203	No change
J2	0.4417	No change
J3	1.4929	No change
J4	25.24	No change

CHAPTER 6 — REFERENCES

AASHTO, Mechanistic-Empirical Pavement Design Guide, Interim Edition: A Manual of Practice, Publication Number AASHTO MEPDG-1, Washington, DC, 2008.

AASHTO, Guide for the Local Calibration of the Mechanistic-Empirical Pavement Design Guide, Publication Number AASHTO LCG-1, Washington, DC, 2010.

AASHTO, Pavement ME Design™ website: http://www.me-design.com/MEDesign/Index.html, 2015.

ARA, *Characterizing Wyoming Traffic for Mechanistic-Empirical Pavement Design*, Draft Final Report submitted to WYDOT, Wyoming Department of Transportation, Cheyenne, Wyoming, September 2012.

ARA, *Characterization of Material Properties for M-E Pavement Design in Wyoming*, Draft Final Report, Subcontractor to University of Wyoming, University of Wyoming ID – 1001898, September 10, 2015.

Bayomy, F., S. El-Badawy, and A. Awed, *Implementation of the MEPDG for Flexible Pavements in Idaho*. Research Report RP 193, University of Idaho, Idaho Department of Transportation, Boise, ID, October 2011.

Darter, M.I., L. Titus-Glover, and H.L. Von Quintus, *Implementation of the Mechanistic-Empirical Pavement Design Guide in Utah: Validation, Calibration, and Development of the UDOT MEPDG User's Guide*, Report No. UT-09.11, Utah Department of Transportation, Research and Materials Division, Salt Lake City, Utah, October 2009.

Darter, Michael I., Jagannath Mallela, Leslie Titus-Glober, Biplab Bhattacharya, and Harold L. Von Quintus, *Calibration and Implementation of the AASHTO Mechanistic-Empirical Pavement Design Guide in Arizona*, Report Number FHWA-AZ-14-606, Project Number SPR 606, Arizona Department of Transportation, Phoenix, Arizona, September 2014.

Mallela, J., Titus-Glover, L., Sadasivam, S., Bhattacharya, B.B., Darter, M.I., Von Quintus, H., *Implementation of the AASHTO Mechanistic-Empirical Pavement Design Guide for Colorado*, Final Report CDOT-2013-4, Colorado Department of Transportation, Denver, Colorado, 2013.

NCHRP, *Development of the 2002 Guide for the Design of New and Rehabilitated Pavement Structures*, Final Report and Software (version 0.70), NCHRP Project 1-37A, Transportation Research Board, Washington, DC, April, 2004.

National Cooperative Highway Research Program, *Changes to the Mechanistic-Empirical Pavement Design Guide Software Through Version 0.900,* NCHRP Research Results Digest 308, NCHRP Project 1-40D, Transportation Research Board, National Research Council, Washington, DC, 2006.

Sachs, S., J. Vandenbossche, M. Snyder, *Developing Recalibrated Concrete Pavement Performance Models for the Mechanistic-Empirical Pavement Design Guide*, NCHRP Project 20-07, Task 327, Transportation Research Board, 2014.

Von Quintus, H.L. and Jim Moulthrop, *Mechanistic-Empirical Pavement Design Guide Flexible Pavement Performance Prediction Models for Montana*, Montana Department of Transportation, 2007.

Von Quintus, H.L., J. Mallela, and L. Titus-Glover, *Calibration Factors for Polymer Modified Asphalts Using M-E Based Design Methods*, Report Number 17985-1/1, Applied Research Associates, Inc., Prepared for the Affiliate Committee of the Asphalt Institute, Lexington, Kentucky, December 2007.

Von Quintus, Harold L. and Rohan Perera, *Extending the Life of Asphalt Pavements*, Report #RC-1551, Michigan Department of Transportation, Office of Research and Best Practices, Lansing, Michigan; May 2011.

Von Quintus, H.L., J. Mallela, R. Bonaquist, C.W. Schwartz, R.L. Carvalho, *Calibration of Rutting Models for Structural and Mix Design*, NCHRP Report No. 719, National Cooperative Highway Research Program, Transportation Research Board, Washington, DC, 2012. http://onlinepubs.trb.org/onlinepubs/nchrp/nchrp_rpt_719.pdf

Von Quintus, H.L., M.I. Darter, B. Bhattacharya, and L. Titus-Glover, *Implementation and Calibration of the MEPDG in Georgia*, Report Number FHWA/GA-014-11-17, Georgia Department of Transportation, Federal Highway Administration, Atlanta, Georgia, June 2015.

WYDOT, Standard Specifications for Road and Bridge Construction. State of Wyoming Department of Transportation, Cheyenne, WY, 2010.